Arabidopsis vascular complexity and connectivity controls PIN-FORMED1 dynamics and lateral vein patterning during embryogenesis

Makoto Yanagisawa, Arthur Poitout, Marisa Otegui

▶ **To cite this version:**

Makoto Yanagisawa, Arthur Poitout, Marisa Otegui. Arabidopsis vascular complexity and connectivity controls PIN-FORMED1 dynamics and lateral vein patterning during embryogenesis. Development (Cambridge, England), 2021, 10.1242/dev.197210 . hal-03264680

HAL Id: hal-03264680
https://hal.inrae.fr/hal-03264680

Submitted on 11 May 2022

HAL is a multi-disciplinary open access archive for the deposit and dissemination of scientific research documents, whether they are published or not. The documents may come from teaching and research institutions in France or abroad, or from public or private research centers.

L'archive ouverte pluridisciplinaire **HAL**, est destinée au dépôt et à la diffusion de documents scientifiques de niveau recherche, publiés ou non, émanant des établissements d'enseignement et de recherche français ou étrangers, des laboratoires publics ou privés.

Distributed under a Creative Commons Attribution 4.0 International License

© 2021. Published by The Company of Biologists Ltd | Development (2021) 148, dev197210. doi:10.1242/dev.197210

RESEARCH ARTICLE

Arabidopsis vascular complexity and connectivity controls PIN-FORMED1 dynamics and lateral vein patterning during embryogenesis

Makoto Yanagisawa[1,2], Arthur Poitout[1,3] and Marisa S. Otegui[1,2,*]

ABSTRACT

Arabidopsis VASCULATURE COMPLEXITY AND CONNECTIVITY (VCC) is a plant-specific transmembrane protein that controls the development of veins in cotyledons. Here, we show that the expression and localization of the auxin efflux carrier PIN-FORMED1 (PIN1) is altered in *vcc* developing cotyledons and that overexpression of PIN1-GFP partially rescues vascular defects of *vcc* in a dosage-dependent manner. Genetic analyses suggest that VCC and PINOID (PID), a kinase that regulates PIN1 polarity, are both required for PIN1-mediated control of vasculature development. VCC expression is upregulated by auxin, likely as part of a positive feedback loop for the progression of vascular development. VCC and PIN1 localized to the plasma membrane in pre-procambial cells but were actively redirected to vacuoles in procambial cells for degradation. In the *vcc* mutant, PIN1 failed to properly polarize in pre-procambial cells during the formation of basal strands, and instead, it was prematurely degraded in vacuoles. VCC plays a role in the localization and stability of PIN1, which is crucial for the transition of pre-procambial cells into procambial cells that are involved in the formation of basal lateral strands in embryonic cotyledons.

KEY WORDS: VCC, PIN1, Lateral vein, Procambial cell specification, Cotyledons

INTRODUCTION

The vascular system is essential for land plants by providing mechanical support and transporting water, nutrients and signaling molecules. There are two main vascular tissues, the xylem, which transports water and minerals, and the phloem, which redistributes sugars produced by photosynthesis and other organic molecules (Lucas et al., 2013). Leaves usually present complex vein networks that become more intricate as the leaf blade expands (Scarpella et al., 2006). The formation of new three-dimensional systems of veins consisting of xylem and phloem is challenging in two ways from a functional point of view: vein networks need to efficiently supply large organs (complexity) and be connected to previously formed veins in such a way that transport is possible from the youngest deeper root all the way to the tallest branch and leaves (connectivity).

The basic pattern of vein architecture is first established during embryo development and after seed germination when xylem and phloem differentiate from procambial cells (Sieburth, 1999). Cotyledons of *Arabidopsis thaliana* embryos are an ideal model system to study vasculature development as they have simple vein patterns with a single middle vein and up to four lateral veins, forming three or four closed loops or areoles (Carland et al., 1999). The vascular patterns defined by procambial strands in embryonic cotyledons remain largely unchanged during post-germination growth when these strands differentiate into mature veins (Sieburth, 1999). However, although several genes are known to control vascular development in embryonic cotyledons (Carland et al., 1999; Koizumi et al., 2000), how procambial strand patterning is determined is not fully understood.

The phytohormone auxin is a key regulator of vascular differentiation and patterning in all organs. The AUXIN RESPONSE FACTOR5/MONOPETEROS (ARF5/MP) controls expression and polarity of the auxin efflux carrier PIN-FORMED1 (PIN1) during vascular formation (Wenzel et al., 2007; Bhatia et al., 2016). Polar localization of PIN1 determines the direction of auxin flow (Wiśniewska et al., 2006), and thus, auxin, ARF5/MP and PIN1 establish a positive feedback loop to amplify auxin signaling (Ohashi-Ito and Fukuda, 2014). During leaf development, PIN1 is expressed in pre-procambial cells before their transition to procambial cells (Scarpella et al., 2006). PIN1 is initially expressed in a group of ground cells and localizes to the plasma membrane with no detectable polarity (Scarpella et al., 2006). Later, its expression is restricted to pre-procambial cell files, and its plasma membrane localization becomes polarized, consistent with its role facilitating auxin flow (Scarpella et al., 2006; Wenzel et al., 2007). These PIN1^{+} cell files developed into procambium (Scarpella et al., 2006).

Consistent with the central role of PIN1 in vascular specification, mutations in proteins that regulate PIN1 localization or expression affect vascular development (Steinmann et al., 1999; Christensen et al., 2000; Benjamins et al., 2001; Geldner et al., 2003; Koizumi et al., 2005). For example, *Arabidopsis* mutants for PINOID (PID), the serine-threonine kinase that regulates PIN polarity by phosphorylation (Friml et al., 2004; Kleine-Vehn et al., 2009), develop floral organs with abnormal vasculature (Christensen et al., 2000; Benjamins et al., 2001). Mutants for either the guanine nucleotide exchange factor (GEF) for ADP-ribosylation factor (ARF) GNOM or the ARF-GTPase activating protein (GAP) VASCULAR NETWORK3/SCARFACE (VAN3/SFC, also known as AGD3), both needed for PIN1 trafficking and polar localization, develop cotyledons with fragmented veins (Steinmann et al., 1999; Geldner et al., 2003; Koizumi et al., 2005). Mutations in ARF5/MP

[1]Department of Botany, University of Wisconsin-Madison, Madison, WI 53706, USA. [2]Center for Quantitative Cell Imaging, University of Wisconsin-Madison, Madison, WI 53706, USA. [3]BPMP, University of Montpellier, CNRS, INRAE, Institut Agro, Montpellier 34060, France.

*Author for correspondence (otegui@wisc.edu)

M.Y., 0000-0002-0918-6169; A.P., 0000-0003-4228-9351; M.S.O., 0000-0003-4699-6950

Handling Editor: Ykä Helariutta
Received 23 September 2020; Accepted 14 June 2021

Development (2021) 148, dev197210. doi:10.1242/dev.197210

result in severe defects in vascular formation in cotyledons (Berleth and Jurgens, 1993; Hardtke and Berleth, 1998), and consistently, lack of function of the transcription factor LONESOME HIGHWAY (LHW), which regulates the proper expression of ARF5/MP, PIN1 and auxin and cytokinin biosynthetic genes, results in vascular development defects in embryos and roots (De Rybel et al., 2013; Ohashi-Ito et al., 2013, 2019; De Rybel et al., 2014; Smet et al., 2019). More than 100 genes are induced by ARF5/MP at the globular stage embryo when procambial cell specification is initiated (Möller et al., 2017), evidencing the complexity of the regulatory gene network underlying auxin-dependent vascular development.

VASCULAR COMPLEXITY AND CONNECTIVITY (VCC) controls vascular patterns in cotyledons (Roschzttardtz et al., 2014) and bilateral leaf symmetry in *Arabidopsis* (Wilson-Sánchez et al., 2018). VCC is a member of the domain of unknown function 1218 (DUF1218) family that includes plant-specific proteins with four predicted transmembrane domains (Roschzttardtz et al., 2014). Other members of the DUF1218 protein family are also involved in vascular-related developmental processes, such as xylem formation (Ubeda-Tomas et al., 2007) and regulation of lignin content and composition in *Arabidopsis* (Mewalal et al., 2016). VCC interacts with OCTOPUS (OPS) (Roschzttardtz et al., 2014), a polarly localized plasma membrane-associated protein needed for phloem development (Truernit et al., 2012; Breda et al., 2019), but its molecular mechanisms of action are unknown.

In this article, we examined PIN1 expression and localization patterns in cotyledons of wild-type and *vcc* embryos. Our data indicate that VCC is required for the proper localization and stability of PIN1 in cell domains specifically involved in the formation of basal lateral veins in embryonic cotyledons.

RESULTS

Vein pattern analysis in wild-type and *vcc* cotyledons

To facilitate the analysis of vein patterns in *Arabidopsis* cotyledons, we used descriptive categories that consider both vein network complexity and connectivity (Fig. 1A; Roschzttardtz et al., 2014). These categories reflect the number of closed areoles (2 to 4) followed by the number of open basal areoles (0 to 2). Basically, as the two distal areoles are present in all vein networks, the variation reflects the presence of basal veins and whether they extend to the middle vein forming closed basal areoles. We also considered separately three types of vein connectivity defects: open distal areoles with at least one gap/disconnection in the distal veins, basal free ends with basal veins disconnected from distal veins, and basal gaps with at least one gap/disconnection in basal veins (Fig. 1A). We quantified the occurrence of each vein network complexity pattern in wild-type and *vcc* cotyledons (Fig. 1B), and through a Pearson's χ^2 analysis determined that the proportions of these categories were significantly different for both phenotypes (χ^2=91.12; d.f.=1; P<2.2e-16). We next clustered the vein network complexity patterns into two groups, i.e. 'complex' (the sum of all vein networks with two basal veins: 4-0, 3-1, 2-2) versus 'simple' (the sum of all vein networks with one or no basal veins: 3-0, 2-1, 2-0), and performed a Pearson's χ^2 test with Yate's continuity correction to compare wild-type and *vcc* cotyledons. Here again, we found significant differences between the two genotypes (χ^2=91.12; d.f.=1; P<2.2e-16), with an increased in 'simple' vein network patterns in *vcc* cotyledons. Finally, we analyzed the occurrence of vein discontinuities [the sum of open distal areoles (oda), basal free ends (bfe) and basal gaps (bga)] and found it to be significantly higher in the *vcc* cotyledons (χ^2=27.044; d.f.=1; P=1.989e-07). To determine whether the predominance of simple vein networks, and therefore reduced basal vein formation in *vcc*, correlate with abnormal cotyledons, we measured cotyledon shape (circularity and roundness) and size in seedlings at 8 days after germination and found no significant differences (Fig. S1), suggesting that VCC role in cotyledon formation is specific to vasculature development.

To better understand the basis of the reduced formation of basal veins and vein patterning defects, we analyzed geometric aspects of the vein networks in wild-type and *vcc* cotyledons. We considered a

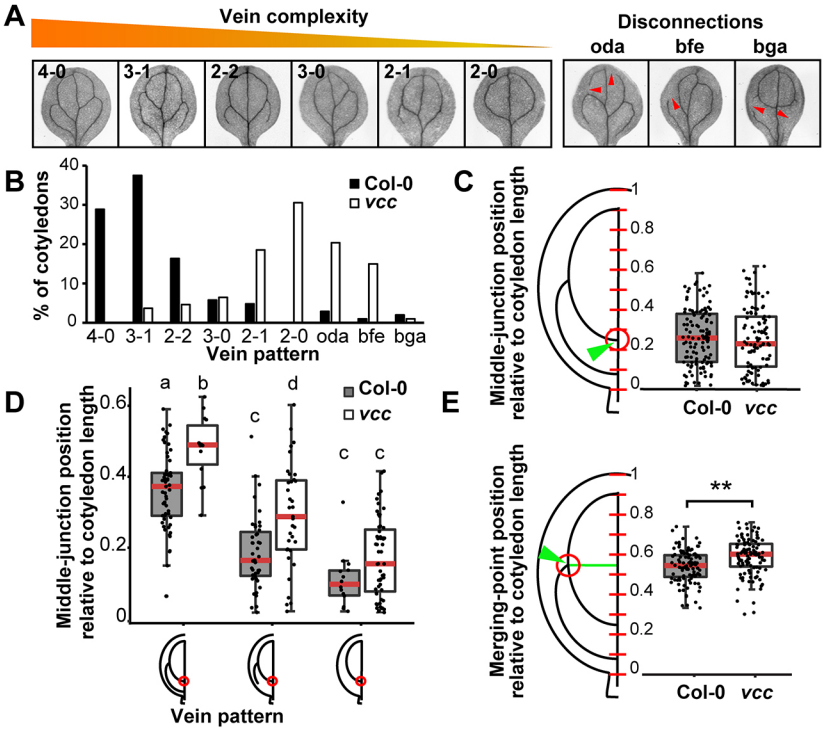

Fig. 1. Analysis of vein pattern and geometry in seedling cotyledons. (A) Vein patterns in cotyledons. The number of closed areoles followed by the number of free-ending basal strands were used for the classification. Vein disconnections include open distal areoles (oda), basal free ends (bfe) and basal gaps (bga). Red arrowheads indicate vein gaps. (B) Vein patterns in wild-type and *vcc* cotyledons (n>100). (C) Position of middle junctions relative to cotyledon length. n>100, P=0.44 (Wilcoxon test). Arrowhead indicates the middle junction point. (D) Position of middle junctions in cotyledons with different vein patterns. Different letters indicate significant differences. n>100, P<0.01 (ANOVA with Tukey's honestly significant difference test). (E) Distribution of merging points relative to cotyledon length. Arrowhead indicates the merging point. n=100, **P<0.01 (Wilcoxon test) in C-E, the red lines indicate the median, the boxes show the upper and lower quartiles, the whiskers indicate the highest and lowest values, and the points represent individual measurements, including potential outliers.

Development (2021) 148, dev197210. doi:10.1242/dev.197210

vein network consisting of a middle vein, two distal and two basal lateral veins, and defined the position of the apical, middle and basal junction points between lateral and middle veins, and the merging point for the lateral (basal and distal) veins (Fig. S2), relative to the cotyledon length. These four points are only present in cotyledons with basal areoles, whereas simpler vein patterns, such as those consisting of two apical areoles (e.g. 2-0), only have apical and middle-junction points. As a single cotyledon can show different lateral vein patterns at each side of the middle vein, we analyzed vein patterning in each cotyledon half independently. We found that in both wild-type and *vcc* cotyledons, the mean middle-junction point was located between 1/5 and 1/3 of the basal portion of the cotyledon length, and was always at a more basal (closer to the petiole) position than the merging point (Fig. 1C). To understand how the position of the middle junction is affected by the overall vein network geometry, we measured the position of the middle junction relative to the cotyledon length in cotyledons with closed apical and basal areoles, closed apical but open basal areoles, or closed apical areole with no basal lateral vein (Fig. 1D). As a general trend in both wild-type and *vcc* samples, we observed a displacement of the middle junction towards more basal positions in vein patterns in which basal veins either did not merge with the middle vein or were absent altogether (Fig. 1D). If low complexity vein patterns correlate with a more basal position of the middle junction, the *vcc* mutant cotyledons would show an overall displacement of the middle junction to more basal positions compared with wild type. However, the opposite was true for *vcc* cotyledons with basal lateral veins, either open or closed (Fig. 1D), suggesting that the misplacement of the middle junction does not explain the reduced vein network complexity of the *vcc* mutant cotyledons. We then analyzed the position of the merging point between basal and apical lateral veins; we found that the average merging point location with respect to cotyledon length was 0.54 for wild type and 0.59 in *vcc* (Fig. 1E), indicating that the position of the merging point between lateral veins is in a more distal position (further away from the petiole) in the *vcc* mutant cotyledons.

Procambial strand patterning in embryonic cotyledons

To determine the timing of procambial strand patterning in cotyledons, we examined developing wild-type embryos expressing *pPIN1::PIN1-GFP* (Benková et al., 2003), which is expressed in pre-procambial cells (Scarpella et al., 2006). Consistent with previous reports (Steinmann et al., 1999; Izhaki and Bowman, 2007; Ploense et al., 2009), PIN1 was detected in all cells of the globular embryo, except the hypophysis, and its expression became restricted to protodermal and pre-procambial cells at heart and torpedo stages (Fig. 2A). In early torpedo embryos, the pre-procambial middle strand was clearly visible in each cotyledon, but the lateral pre-procambial strands were not detectable at this stage (Fig. 2A). At the early bent-cotyledon stage, PIN1-GFP was no longer detectable in the epidermis but restricted to procambial cells. At this stage, middle and lateral procambial strands were already established with patterns similar to those seen in the cotyledons of germinating seedlings (Fig. 2A). These results suggest that the formation of lateral procambial strands in cotyledons occurs between the torpedo and early bent-cotyledon stages.

We then analyzed cotyledons in the developmental window between early torpedo and early bent cotyledon. We identified several intermediate pre-procambial and procambial strand patterns,

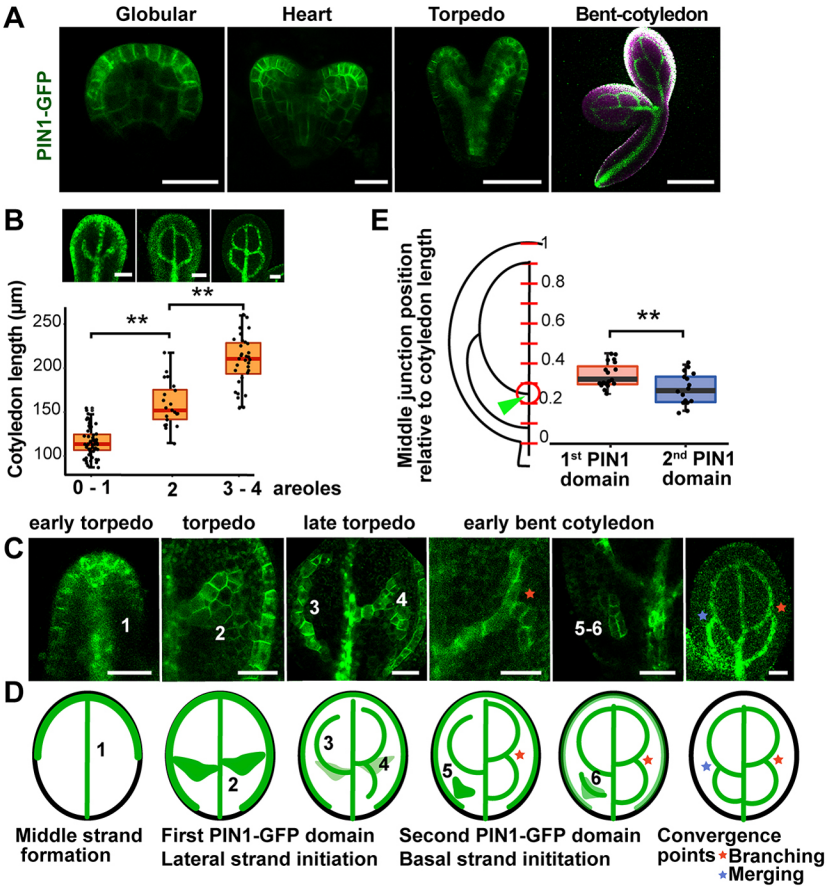

Fig. 2. Lateral strand formation in embryonic cotyledons. (A) Expression of PIN1-GFP in embryos. (B) Example images of 0-1, 2 and 3-4 areoles. Analysis of cotyledon length as a function of different developmental stages in lateral strand formation. $n>100$, $^{**}P<0.01$ (ANOVA with Tukey's honestly significant difference test). (C,D) Representative images (C) and corresponding schematic representations (D) of embryonic cotyledons during pre-procambial/procambial strand formation, as evidenced by PIN1-GFP expression. Numbers highlight sequential events. Red and blue asterisks indicate strand branching and merging, respectively. Both events result in the establishment of the merging point. (E) Basal strand formation is affected by the middle-junction position. $n=33$ half cotyledons, $^{**}P<0.01$ (unpaired, two-tailed *t*-test). Green arrowhead indicates the middle junction. Scale bars: 20 µm in globular and heart, 50 µm in torpedo and 200 µm in bent-cotyledon embryos (A); 30 µm (B); 20 µm (C). In B,E, the horizontal lines indicate the median, the boxes show the upper and lower quartiles, the whiskers indicate the highest and lowest values, and the points represent individual measurements, including potential outliers.

Development (2021) 148, dev197210. doi:10.1242/dev.197210

and classified them into three different categories based on the increasing number of areoles, that is 0 to 1 (low complexity), 2 (intermediate complexity), and 3 to 4 areoles (high complexity) (Fig. 2B). There was a positive correlation between procambial pattern complexity and cotyledon length (Fig. 2B), indicating that the complexity of procambial strand networks increases as a function of cotyledon growth.

To further dissect how lateral procambial strands are established, we examined embryonic cotyledons of various lengths between early torpedo and early bent-cotyledon stages (Fig. 2C,D). No lateral strands were detectable in cotyledons up to 70 µm in length (early torpedo stage). When cotyledons were between 70 µm and 120 µm in length (torpedo), PIN1-GFP expression became stronger underneath the epidermis, forming a domain extending from the margin to the middle strand and located approximately at the middle of the cotyledon length. Similar to what has been described previously in leaf primordia (Scarpella et al., 2006; Wenzel et al., 2007), this PIN1 domain originates underneath an epidermal cell in which PIN1-GFP is localized at the anticlinal sides facing the neighboring epidermal cells and the periclinal side towards a subepidermal cell (Fig. 3A). This PIN1 domain became connected to the middle strand, establishing the middle junction (Fig. 2C,D; step 2). When cotyledons were between 120 µm and 160 µm in length (late torpedo), the expression of PIN1-GFP within this domain became restricted to narrow cell files following one of two patterns: (1) a single linear strand that extended towards the apex as the distal strand (Fig. 2C,D; step 3), or (2) a Y-shaped strand with arms extending apically and basally as the distal and basal strands, respectively (Fig. 2C,D; step 4). As these lateral strands extended towards the apex or the petiole, they merged with the middle strand, establishing the apical and the basal junctions, respectively, and closing the areoles. In some cotyledons in which the first PIN1 domain gives rise to only the distal strand, a second PIN1-GFP domain became evident at a more basal position at the early bent-cotyledon stage (Fig. 2C,D; step 5). This second PIN1 domain also formed underneath the epidermis (Fig. 3B), but it was not always clearly related to cells with unusual PIN1 distribution. PIN1 expression became restricted to a file of short isodiametric pre-procambial cells that extended upwards, merging with the distal strand and basally with the middle strand (Fig. 2C,D; step 6). In the cell located at the merging point, PIN1-GFP was localized at the sides perpendicular to the strand, as well as at the side in contact with the basal strand (Fig. 3C). We confirmed that the isodiametric cells in developing strands were pre-procambial based on their ability to express the pre-procambial marker *pATHB8::NLS-YFP* (Sawchuk et al., 2007) (Fig. 3D,E). Procambial strand patterning was complete in cotyledons longer than 200 µm at the bent-cotyledon stage.

Basal strands form either simultaneously with distal strands from the first PIN1 domain or from the second PIN1 domain after distal strand initiation (Fig. 2D). This means that the merging point between lateral strands is established early in the first case but later in the second case.

We then determined whether the mechanism by which the merging point is established affects other vein patterning features. We found that when the basal strand is originated by the second PIN1 domain, the position of the middle junction is located at a more basal position than when the basal strand originates from branching of the first PIN1 domain (Fig. 2E).

PIN1 expression pattern is altered in *vcc* embryonic cotyledons

To determine how VCC regulates lateral strand formation, we analyzed the expression of PIN1-GFP in *vcc* embryonic cotyledons. We examined embryos with cotyledons longer than 200 µm and already established procambial strands. In these *vcc* developing cotyledons, the procambial strand networks revealed the same trend of low complexity, with reduced occurrence of basal strands (Fig. 4A,B), similar to what was seen in *vcc* seedling cotyledons after germination (Fig. 1B). The presence of basal strands was observed in 97% of wild-type (n=68) and 65% of *vcc* (n=96) embryonic cotyledons at the bent-cotyledon stage (longer than 200 µm; Fig. 4C).

We then checked earlier developmental stages to determine the underlying cause of the reduction in basal vein formation. In 120-160 µm-long cotyledons, PIN1-GFP^{+} pre-procambial basal strands were observed in both wild type and *vcc* at comparable frequencies (76% of wild-type cotyledons, n=36; and 78% of *vcc* cotyledons, n=23; Fig. 4C; Fig. S3). However, at a later stage (160-200 µm-long cotyledons), the presence of basal strands was reduced to 70% in *vcc* (n=73) and increased to 82% in wild type (n=72) (Fig. 4C). Consistent with this trend, basal veins occurred in 91% and 34% of cotyledons of wild-type and *vcc* mutant seedlings, respectively (n>500 per genotype; Fig. 4C), suggesting that, although the

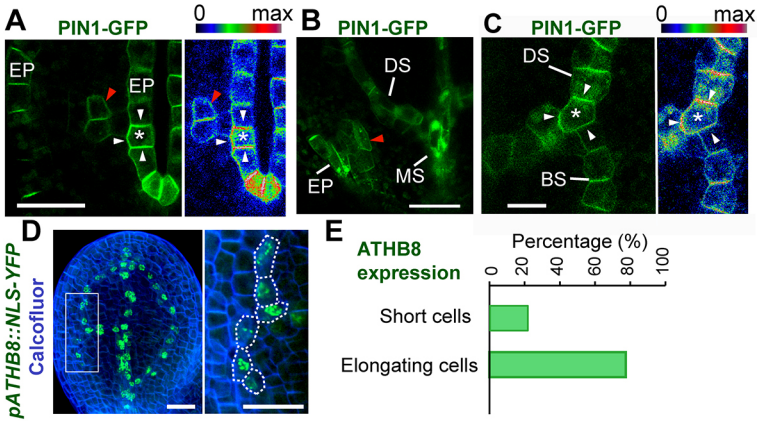

Fig. 3. Formation of PIN1 domains and procambial strands in cotyledons. (A) Formation of the first PIN1 domain (red arrowhead) in association with an epidermal cell (asterisk) in which PIN1 is localized at the anticlinal sides, as well as the side facing the subepidermal layer (white arrowheads). The right panel is pseudocolored according to fluorescence intensity to better visualize PIN1-GFP distribution. Torpedo embryo; cotyledon length: 85 µm. (B) Formation of second PIN1 domain (red arrowhead) in cotyledons (135 µm in length) of a torpedo embryo. (C) Localization of PIN1-GFP (white arrowheads) in the cell located at the merging point (asterisk) between distal (DS) and basal (BS) strands in cotyledons (140 µm in length) of a torpedo embryo. The right panel is pseudocolored according to fluorescence intensity to better visualize PIN1-GFP distribution. (D) Expression of *pATHB8::NLS-YFP* in developing cotyledons of torpedo embryos. Embryos were cleared and stained with calcofluor to visualize cell walls. The area contained within the white box is enlarged in the right panel. (E) Bar graph showing the percentage of short (length <1.5× width) and elongating cells (length >1.5× width) in developing basal strands expressing *pATBH8::NLS-YFP* (n=200 cells). EP, epidermis; MS, middle strand. Scale bars: 20 µm.

Development (2021) 148, dev197210. doi:10.1242/dev.197210

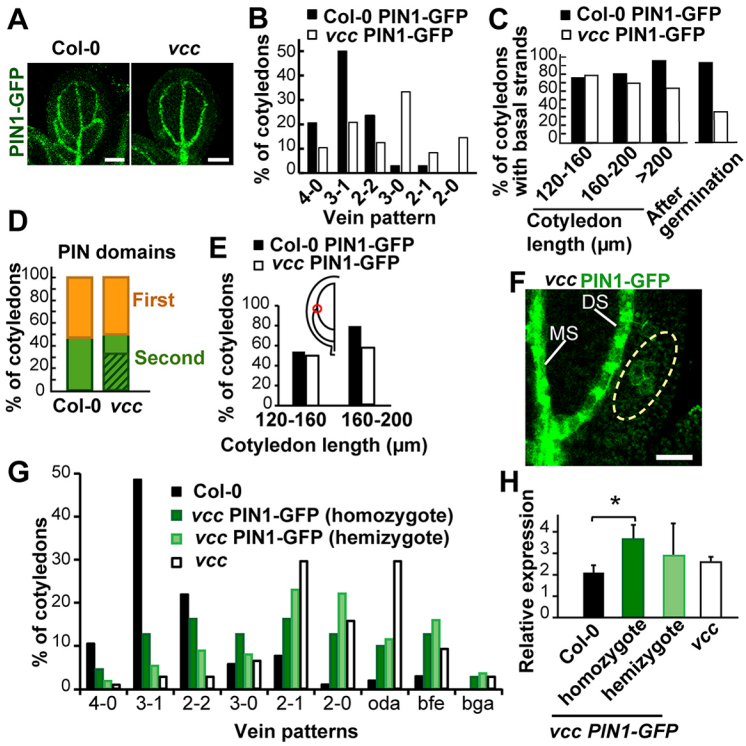

Fig. 4. Lateral strand formation in *vcc* embryos. (A) PIN1-GFP expression patterns in wild-type and *vcc* cotyledons (>200 µm in length). (B) Procambial strand patterns in wild-type and *vcc* in cotyledons longer than 200 µm (n=34 in Col-0, n=48 in *vcc*). (C) Occurrence of basal strands in cotyledons at different developmental stages and in seedlings of wild-type and *vcc* mutant plants. (D) Frequency of basal strands originated from the first (orange) or second (green) PIN1 domains in wild-type and *vcc* cotyledons (120-160 µm in length). The striped region corresponds to the fraction of cotyledons showing weak GFP signal in the second PIN1 domain. (E) Percentage of wild-type and *vcc* cotyledons with established merging points at two different developmental stages. (F) Weak GFP signal at a second PIN1 domain in a *vcc* cotyledon (>200 µm in length). By enhancing the weak GFP signal at the second PIN1 domain, the fluorescence signal from other regions became saturated. Middle strand (MS) and distal strand (DS) are labeled. (G) Distribution of vein patterns in seedling cotyledons. Homozygous and hemizygous PIN1-GFP lines in the *vcc* background were analyzed together with wild type and *vcc*. (H) Relative expression level of PIN1/PIN1-GFP determined by RT-qPCR. *UBQ10* was used as an internal control. Data are mean±s.d. of three biological replicates. *P<0.05 (paired, two-tailed t-test). Scale bars: 50 µm (A); 20 µm (F).

initiation of basal pre-procambial cells proceeds normally in *vcc* mutant embryos, their subsequent specification into procambial strands is compromised.

We found that basal pre-procambial strand initiation originated by either branching from the first PIN1 domain or from the second PIN1 domain occurred at similar rates in wild-type (54% from first PIN1 domain and 46% from second PIN1 domain; n=39) and *vcc* (50% from both first and second PIN1 domain; n=23) cotyledons (Fig. 4D). We also found that in 120-160 µm-long cotyledons, the frequency of merging points generated by the branching of the first PIN1 domain was ∼50% in both wild-type (n=35) and *vcc* (n=22) cotyledons. However, at a later stage (160-200 µm-long cotyledons), the frequency of merging points increased to 80% (n=44) in wild type but remained nearly unchanged (57%, n=39) in *vcc* (Fig. 4E). The increase in the frequency of merging points in wild-type cotyledons was caused by the merging of distal and basal strands originated from the second PIN1 domain, suggesting that this event is compromised in *vcc* cotyledons. Consistent with this observation, in 37% of the *vcc* cotyledons longer than 200 µm, the fluorescent signal from the second PIN1 domain became weaker compared with wild type (Fig. 4D,F), suggesting that basal strand formation by the second PIN1 domain does not progress normally in the *vcc* cotyledons. The premature disappearance of the second PIN1 domain would explain the reduced occurrence of basal veins seen in *vcc* cotyledons (Fig. 4B).

These transgenic *vcc* plants were generated by crossing with a Col-0 line expressing *pPIN1::PIN1-GFP* (Benková et al., 2003). We expected that the resulting *vcc pPIN1::PIN1-GFP* line would have the same vasculature defects seen in *vcc* cotyledons. However, the reduction in vein network complexity in *vcc* embryonic cotyledons expressing PIN1-GFP (Fig. 4B) was less pronounced than that observed in *vcc* seedlings (Fig. 1B). Thus, whereas the most complex 4-0 and 3-1 vein network patterns represented less than 5% of the *vcc* seedling cotyledons (Fig. 1B), those same patterns were seen in ∼30% of the *vcc* embryonic cotyledons expressing PIN1-GFP (Fig. 4B). We hypothesized that the overexpression of PIN1 caused by the introduction of *pPIN1::PIN1-GFP* in *vcc* has an effect on vein network complexity. To test this, we analyzed cotyledon vein patterns in *vcc* seedlings expressing different levels of *PIN1-GFP* during embryo development. We found a positive correlation between the partial restoration of vein network complexity in *vcc* cotyledons and increasing levels of *PIN1*/*PIN1-GFP* expression (Fig. 4G,H).

Mutations in *PIN1* and *PINOID* differentially affect vein connectivity in *vcc* cotyledons

As we found a functional connection between VCC and PIN1, we examined vein patterns in the *pin1-1* single mutant. As previously reported, the *pin1* mutant exhibited embryos with two fused cotyledons, or only one or three free cotyledons (Aida et al., 2002). We also considered the occurrence of fused cotyledons in our analysis (Fig. 5A). Approximately 7% of the *pin1-1* cotyledons show reduced and distorted areoles closed to the cotyledon apex (Fig. 5A). Although we did not determine the origin of these abnormal areoles, for the purpose of our analysis, we considered them as distal areoles based on their position. Both *pin1-1* and *vcc* showed reduced vascular network complexity and connectivity in seedling cotyledons at similar rates (Fig. 5A).

To better understand genetic interaction between *VCC* and *PIN1*, we generated a *vcc pin1-1* double mutant by crossing. We performed a pairwise χ^2 test between all genotypes comparing the occurrence of ‘complex’ versus ‘simple’ patterns, and calculated false discovery rates to adjust P-values. We concluded that whereas the two wild-type ecotypes used as control have a similar proportion of complex and simple patterns, all three mutants (*pin1-1*, *vcc*, and *pin1-1 vcc*) showed a significant increase in simple vein network patterns compared with both wild types. However, the proportion of simple versus complex patterns in the three mutants was similar (Fig. 5A; Table S1), with only *vcc pin1-1* versus *vcc* showing a slightly significant increase in the occurrence of simple patterns

Development (2021) 148, dev197210. doi:10.1242/dev.197210

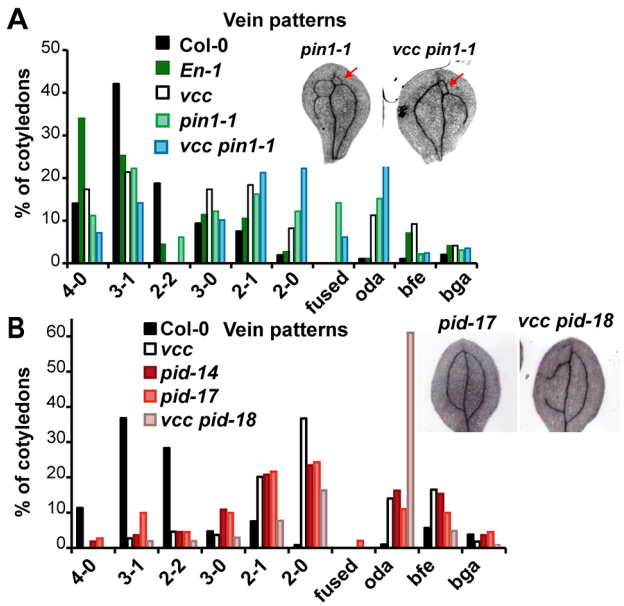

Fig. 5. Double mutant analysis. (A) Frequency of vein patterns in Col-0, En-1, *vcc*, *pin1-1* and *vcc pin1-1*. Representative images of distorted distal areoles (red arrows) in *pin1-1* and *vcc pin1-1* cotyledons. (B) Frequency of vein patterns in Col-0, *vcc*, *pid-17* and *vcc pid-18*. Representative images of *pid-17* and *vcc pid-18* cotyledons.

(adjusted P=0.04). In terms of the occurrence of vein disconnections, we found no statistically significant differences between either *vcc* and *pin1-1* (P=0.86), or between each of the single mutants and the *vcc pin1-1* double mutant (P=0.3 for both cases). However, *pin1-1* and *vcc pin1-1*, but not *vcc* cotyledons, exhibited small abnormal areoles close to the cotyledon apex (Fig. 5A). These results suggest that both PIN and VCC act on the same pathway controlling basal vein formation and vein connectivity in cotyledons, and that combined mutations in *VCC* and *PIN1* do not lead to enhanced vein defects.

PINOID (PID) is a serine-threonine protein kinase that controls the polarity of PIN proteins at the plasma membrane (Christensen et al., 2000; Friml et al., 2004), which is known to affect vascular patterning (Kleine-Vehn et al., 2009). To test whether there is a genetic interaction between *VCC* and *PID*, we decided to generate *vcc pid* double mutants. However, as *PINOID* (At2g34650) and *VCC* (At2g32280) are located fairly close to each other in chromosome 2, we were unable to generate double mutants by crossing *vcc* with existing *pid* mutants. Instead, using CRISPR/Cas9 technology (Wang et al., 2015), we generated *pid* mutations in wild-type Col-0 and *vcc* plants. Although we were unable to isolate identical *pid* mutations in both genetic backgrounds, we found in both lines a single nucleotide insertion at position 233 (G in the Col-0 and T in *vcc*) after the translation start site that causes a codon reading frame shift after amino acid 78 of the PID protein. Although the two resulting *pid* alleles are not identical, their deduced translated protein products are (Fig. S4). We named these new alleles *pid-17* and *vcc pid-18* (Fig. S4). Seedlings homozygous for the *pid-17* mutation commonly exhibited three cotyledons and were used for vein pattern analysis. We also analyzed the already characterized *pid-14* mutant (Haga et al., 2014) as a reference. We found a statistically significant difference between wild type and the four mutant lines (*pid14*, *pid-17*, *vcc* and *vcc pid-18*) in terms of proportion of 'complex' versus 'simple' vein network patterns in cotyledons (Fig. 5B; Table S1). In addition, in pairwise χ^2 analyses using false recovery rates, we found no significant differences in the proportion of vein network complexity patterns among the four mutant lines (P>0.05 for all pairwise comparisons; Table S1). However, the *vcc pid-18* double mutant showed a significantly higher proportion of vein disconnections compared with either single mutant (P<0.0001 in both cases). In fact, compared to the single mutants, the *vcc pid-18* cotyledons had a sixfold increase in the occurrence of open distal areoles (Fig. 5B). These results are consistent with both VCC and PID acting with PIN1 through a common mechanism to determine basal strands in cotyledons. However, the drastic increase in distal vein gaps in the double mutants suggests that VCC and PID may control distal vein connectivity in a partially or completely independent manner.

Auxin induces *VCC* expression

VCC has been reported as one of the ARF5/MP target genes during the globular embryo stage (Möller et al., 2017). ARF5 recognizes the auxin-response elements TGTCTC (Ulmasov et al., 1995) and TGTCGG (Boer et al., 2014), promoting gene expression in the presence of auxin. We searched the *VCC* promoter region and found the auxin-response element TGTCTC in reverse orientation (GACACA) at the −260 position from the transcription start site. Neither a TGTCTC nor a GACACA sequence necessarily implies the presence of an auxin-responsive element. In fact, nearly half of *Arabidopsis* genes contain these sequences within 1000 base pairs from the transcriptional site (Mironova et al., 2014). Therefore, we measured the steady-state level of *VCC* transcripts in seedlings treated with synthetic auxin NAA by RT-PCR and RT-qPCR (Fig. 6A,B). *VCC* transcripts were significantly increased after 24 h of auxin treatment, confirming that auxin induces *VCC* expression.

Expression and subcellular localization of VCC in the root tip

To determine its subcellular localization and expression pattern, we tagged VCC with 3xYPET (3x-YFP) using recombineering technology (Yanagisawa et al., 2018; Brumos et al., 2020), and expressed it in *vcc* mutant plants (Fig. S5). We introduced the 3x-YFP tag at the N-terminal, the C-terminal or the cytoplasmic loop region of VCC, and checked whether the expression of these three

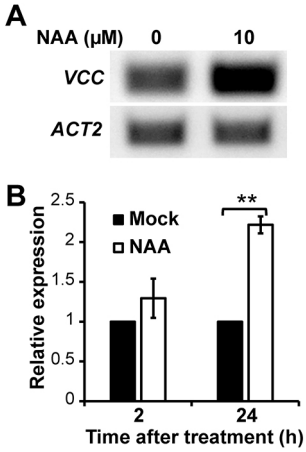

Fig. 6. *VCC* expression analysis after auxin treatment. (A,B) *VCC* expression in 12-day-after-germination seedlings after treatment with 0 μM or 10 μM NAA. (A) RT-PCR analysis of *VCC* transcripts after 24-h NAA treatment. *ACTIN2* was used as an internal control. (B) Relative expression levels of *VCC* were determined by RT-qPCR after 2-h and 24-h NAA treatment. *UBQ10* was used as an internal control. Data are mean±s.d. of three biological replicates. **P<0.01 (paired, two-tailed *t*-test).

Development (2021) 148, dev197210. doi:10.1242/dev.197210

tagged versions was able to rescue the cotyledon vein defects of the *vcc* mutant (Fig. S5B,C). We found that the expression of C-terminally and N-terminally tagged VCC partially rescued both the complexity and connectivity vein defects of the *vcc* mutant cotyledons (Fig. S5C).

Previously, we reported the expression of *VCC* in embryos, developing vasculature of roots and cotyledons, anthers, and the vascular cambium of the hypocotyl of mature *Arabidopsis* plants (Roschzttardtz et al., 2014). Although the *vcc* mutant does not have detectable root developmental defects, *VCC* expression in the root tip is relatively high, and consistently, we detected a strong 3x-YFP-VCC signal in the root meristematic region. As roots are ideal for confocal imaging of deep tissues, where VCC is mostly expressed, we decided to analyze the subcellular localization of 3x-YFP-VCC in root cells. We observed 3x-YFP fluorescent signal in cortex, endodermis and stele of the root meristematic zone (Fig. 7A,B). The subcellular localization varied among these cell types; although in all cells 3x-YFP-VCC was detected at the cell periphery, in the endodermal and vascular cells, it was also localized to large organelles reminiscent of vacuoles (Fig. 7B). To unambiguously determine the localization of 3x-YFP-VCC, we stained transgenic seedlings with FM4-64 to label the plasma membrane (Fig. 7C), and introduced the tonoplast marker VAMP711-mCherry (Geldner et al., 2009) by crossing (Fig. 7E). Signal intensity profiles revealed that 3x-YFP-VCC and FM4-64 signals overlap at the plasma membrane of cortex, endodermal and vascular cells, whereas the internal signal seen in meristematic endodermal and vascular cells corresponds to the vacuolar lumen (Fig. 7D,F). We did not find evidence of polar distribution of 3x-YFP-VCC at the plasma membrane of root cells.

VCC and PIN1 dynamics in embryonic cotyledons

To analyze the dynamics of both VCC and PIN1 expression and localization in embryos during pre-procambial fate determination, we generated seedlings expressing *pPIN::PIN1-GFP* and *pVCC::tdTomato-VCC*. VCC was expressed strongly in vascular cells and weakly in the ground cells at the globular stage (Fig. 8A). From heart to torpedo stages, VCC was detected in pre-procambial and procambial cells, and surrounding ground cells (Fig. 8A). At the early bent-cotyledon stage, both VCC and PIN1 were expressed in the central procambial strand of the embryo axis and in middle and lateral strands of cotyledons, with a weaker expression of VCC in cotyledon ground cells (Fig. 8A).

During the formation of the first PIN1 domain, VCC was expressed ubiquitously in ground cells but more strongly in the elongating cells of the middle procambial strand (Fig. 8B). At this stage (110 µm long-cotyledons), VCC and PIN1 were localized to the plasma membrane and cytoplasmic puncta in ground cells but also to the vacuolar lumen of the procambial cells in the middle strand (Fig. 8B; Fig. 9A,B). As the expression of PIN1-GFP intensified in developing lateral strands and pre-procambial cells started to elongate, transitioning into procambial cells (170-µm-long cotyledons), the tdTomato-VCC signal also became stronger in these cells and was redistributed together with PIN1-GFP from the plasma membrane to the vacuolar lumen (Fig. 8B; Fig. 9C,D).

To further confirm that the sequestration of VCC into vacuoles was preferentially occurring in PIN1-GFP^{+} procambial cells, we calculated the ratio of tdTomato-VCC signal between the interior (intracellular, mostly vacuolar) and the plasma membrane of ground cells devoid of PIN1-GFP, and in procambial cells strongly expressing PIN1-GFP1. We found a statistically significant increase in the intracellular/vacuolar ratio of VCC signal in procambial cells expressing PIN1-GFP (Fig. 9E), suggesting that VCC is internalized from the plasma membrane and delivered to the vacuole for degradation in cells undergoing procambial fate determination.

We then studied more closely the dynamics of tdTomato-VCC and PIN1-GFP during the transition from pre-procambial to procambial cell fate. The elongation of pre-procambial cells that accompanies their transition into procambial cells is marked by a more pronounced polarization of PIN1 at the plasma membrane (Fig. 9F). VCC also localized to the plasma membrane of pre-procambial cells but did not show detectable polarization (Fig. 9G,H). As the strands continue to extend and pre-procambial cells elongate, VCC was mostly detected inside vacuoles together with PIN1-GFP, suggesting that vacuolar sequestration and degradation of both VCC and PIN1 increase at this stage.

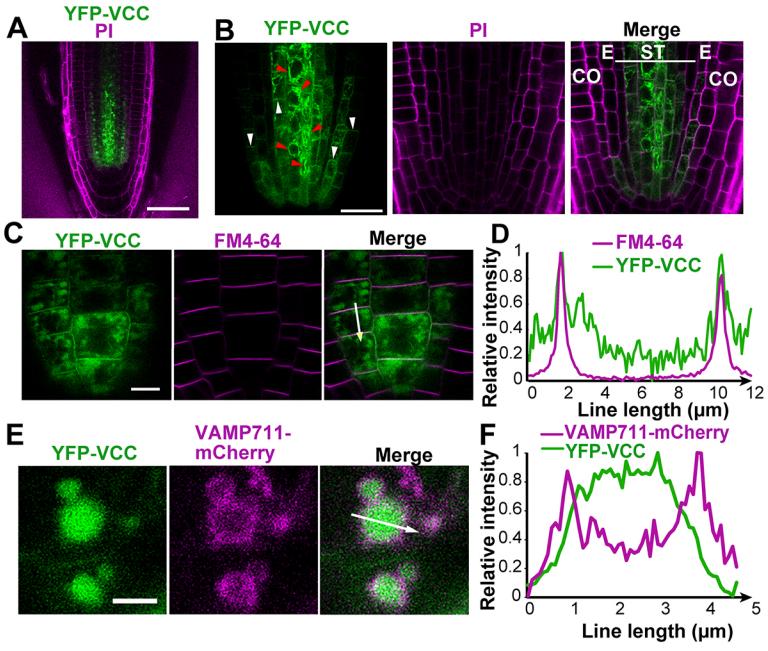

Fig. 7. Expression and subcellular localization of VCC in the root meristematic region. (A) 3x-YFP-VCC expression in the root meristematic zone. (B) Seedlings expressing 3x-YFP-VCC were stained with propidium iodide (PI) to label cell walls. Tissue types are labeled as cortex (CO), endodermis (E) and stele (ST). White arrowheads indicate YFP signal at the cell periphery and red arrowheads indicate YFP signal in large intracellular compartments. (C) Root meristematic region of a seedling expressing 3x-YFP-VCC and stained with FM4-64. (D) Fluorescence intensity profiles of 3x-YFP-VCC and FM4-64 along the arrow depicted in C. (E) Root meristematic region of a seedling expressing both 3x-YFP-VCC and the tonoplast marker VAMP711-mCherry. (F) Fluorescence intensity profiles of 3x-YFP-VCC and VAMP711-mCherry along the arrow depicted in E. Scale bars: 50 µm (A); 20 µm (B); 10 µm (C); 3 µm (E).

Development (2021) 148, dev197210. doi:10.1242/dev.197210

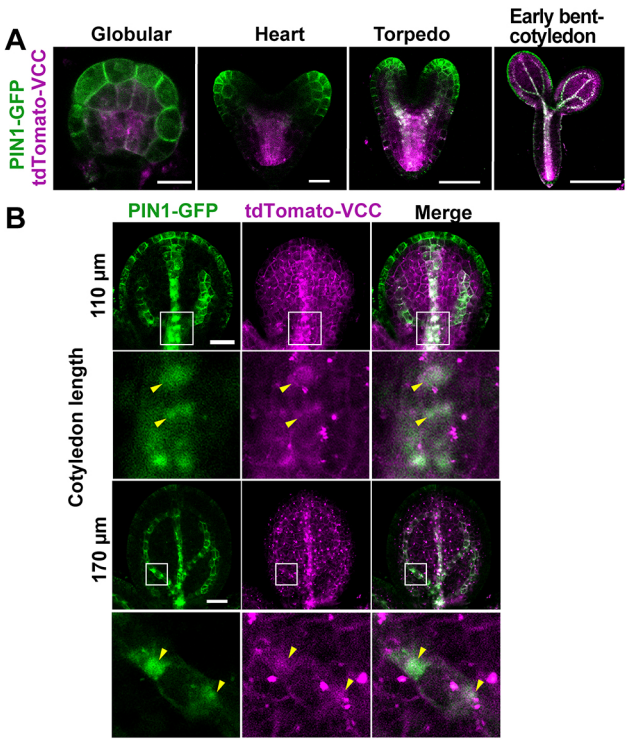

Fig. 8. Expression and localization of VCC and PIN1 in embryos. (A) tdTomato-VCC and PIN1-GFP expression during embryo development. (B) Expression pattern and localization of tdTomato-VCC and PIN1-GFP during lateral strand formation in embryonic cotyledons. Areas contained within the white boxes are enlarged in the panels below. Arrowheads indicate PIN1-GFP and tdTomato-VCC signals inside vacuoles. Scale bars: 10 µm in globular, 20 µm in heart, 50 µm in torpedo and 200 µm in early bent-cotyledon (A); 20 µm (B).

To understand how VCC affects vein patterning through PIN1, we analyzed PIN1 subcellular localization in pre-procambial cells in developing basal strands of 120- to 160-µm-long cotyledons. We noticed that PIN1 polarization was less common in *vcc* pre-procambial cells compared with wild type (Fig. 9J). As basal strands extend and merge with the middle strand and/or the distal strand in 160- to 200-µm-long cotyledons, 98% of the wild-type but only 70% of the *vcc* mutant cotyledons showed polar localization of PIN1 in pre-procambial/procambial cells (Fig. 9I,J). Consistently, at this stage pre-procambial cell expansion was impaired in basal strands of *vcc* mutants (Fig. 9I,J). We also noticed that the vacuolar delivery of PIN1 was accelerated in the *vcc* mutant cotyledons compared with wild type, as vacuolar PIN1-GFP signal was detected at earlier stages in pre-procambial/procambial cells of *vcc* cotyledons (Fig. 9I,J). These results, together with our observation of the transient nature of the second PIN1 domain in *vcc* mutants, suggest that VCC is important for the localization and stability of PIN1 at the plasma membrane during the transition from pre-procambial into procambial cells.

DISCUSSION

The simple and regular vein patterns of *Arabidopsis* cotyledons make them an ideal model system to study vascular development. A relatively large number of mutants have been reported to show vascular patterning defects in seedling cotyledons. The formation of the middle vein seems to be more robust than that of lateral veins as only a few mutants for genes in the early steps in auxin signaling, such as *AXR6/CULLIN1* and *ARF5/MP*, occasionally show abnormal middle veins (Berleth and Jurgens, 1993; Hobbie et al., 2000). For our analysis of lateral veins, we considered two parameters: (1) network complexity, given by the number of closed distal areoles and the presence of basal veins forming either closed or open basal areoles; and (2) connectivity of both distal and basal lateral veins. The two parameters are somehow related as most mutants with defects in vein network complexity also show vein disconnections. Fragmentation of lateral veins is an extreme form of connectivity defect, and it has been reported in mutants for the sterol biosynthesis enzyme COTYLEDON VASCULAR PATTERN1/STEROLMETHYLTRANSFERASE2 (Carland et al., 2002) and for the vesicle trafficking proteins GNOM/VAN7 and VAN3/SFC (Koizumi et al., 2000). Interestingly, FORKED1/VAN3-BINDING PROTEIN (FKD1/VAB) interacts with VAN3/SFC and it is required for establishing the apical junction and merging points (Steynen and Schultz, 2003; Naramoto et al., 2009).

Mutations in *VCC* cause both reduced complexity and connectivity in cotyledon vasculature (Roschzttardtz et al., 2014). Similar vein defects have been reported in mutants for PID (Kleine-Vehn et al., 2009), OPS (Truernit et al., 2012), LHW (Ohashi-Ito and Bergmann, 2007) and an inositol polyphosphate 5′-phosphatase COTYLEDON VASCULAR PATTERN2 (Carland and Nelson, 2009). Except for OPS, all these proteins have been reported to influence PIN1 expression patterns and/or localization (Kleine-Vehn et al., 2009; Naramoto et al., 2009; Ohashi-Ito et al., 2013). Although PID is uniformly localized at the plasma membrane of the root cells (Dhonukshe et al., 2010), its kinase activity is required for proper PIN1 polarization (Friml et al., 2004). Likewise, although VCC itself is not polarized at the plasma membrane (Fig. 9G,H), it does promote polarization of PIN1 in pre-procambial cells, and our analysis of a double *vcc pid* mutant suggests that both VCC and PID are required for PIN1-mediated control of vasculature network complexity. Interestingly, although VCC seems to functionally overlap with PID in the modulation of PIN1 function, VCC is not required for normal cotyledon development, as the *vcc* mutants do not show the fused cotyledons or supernumerary cotyledons typical of *pin1* and *pid* mutants, respectively. Based on genetic studies, the trafficking components VAN3/SFC and FKD1/VAB1 have been hypothesized to act in the same pathway as PID (Sieburth et al., 2006; Hou et al., 2010), suggesting that PIN1 is regulated by multiple partially overlapping pathways during vascular development in cotyledons. VCC physically interacts with OPS (Roschzttardtz et al., 2014), which is a positive regulator of the brassinosteroid pathway and phloem differentiation (Anne et al., 2015), suggesting a role for VCC in the integration of both auxin and brassinosteroid signaling for vascular development in embryos. Cytokinin also controls PIN1 polarization and dynamics. Cytokinin enhances differential internalization of PIN1 from specific cell sides and stimulates its degradation in vacuoles (Marhavý et al., 2011, 2014). Whether VCC is involved in cytokinin signaling to regulate PIN1 dynamics is unknown. However, the polarity defects and premature degradation of PIN1 in *vcc* mutants are consistent with that possibility.

VCC expression is induced by auxin (Fig. 6) and likely controlled by the ARF5/MP transcription factor (Möller et al., 2017). In fact, the expression patterns of *VCC* and *ARF5/MP* during embryo development are similar, with both switching from a broad expression in ground cells to a more restricted expression in pre-procambial/procambial cells during vascular specification (Fig. 8A,B; Hamann et al., 2002; Wenzel et al., 2007). These results are consistent with a role for VCC in vascular development through an auxin positive feedback loop.

Development (2021) 148, dev197210. doi:10.1242/dev.197210

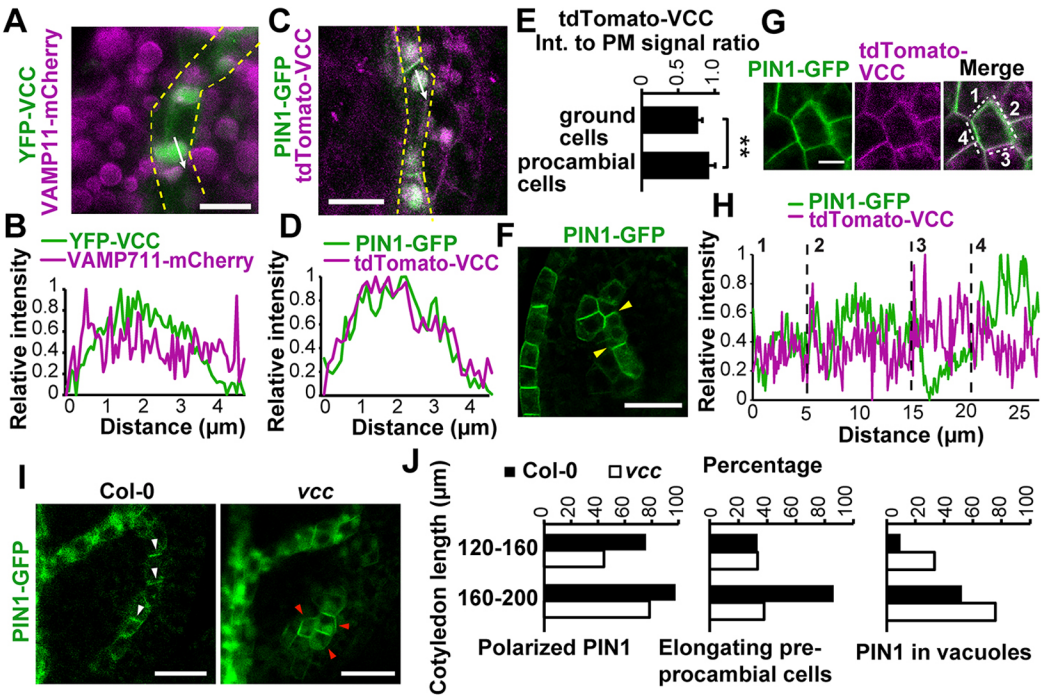

Fig. 9. Subcellular localization analysis of VCC and PIN1 during lateral strand formation. (A-D) Localization of tdTomato-VCC, 3x-YFP-VCC and PIN1-GFP in vacuoles of procambial cells. Signal of 3x-YFP-VCC was detected inside vacuoles labeled with the tonoplast marker VAMP711-mCherry in developing cotyledons (180 µm in length) of torpedo embryos (A,B). td-Tomato-VCC and PIN1-GFP colocalized inside vacuoles in developing cotyledons (175 µm in length) of torpedo embryos (C,D). Yellow broken lines outline procambial cell files. (E) Ratio between intracellular (int) and plasma membrane (PM) tdTomato-VCC fluorescent signal in ground and procambial cells. n=67 for each cell type, $^{**}P$<0.01 (unpaired, two-tailed t-test). Error bars indicate s.d. (F) Representative image of polarized PIN1-GFP in elongating pre-procambial cells in developing cotyledons (115 µm in length) of torpedo embryos. (G,H) Intensity profile analysis of PIN1-GFP and tdTomato-VCC at the plasma membrane of pre-procambial cells. (G) Pre-procambial cells in developing cotyledons (90 µm in length) expressing both PIN1-GFP and tdTomato-VCC. (H) Fluorescence intensity profiles along the dashed-lines with corresponding numbers in G. (I) PIN1-GFP localization in developing basal strands of wild-type and *vcc* embryonic cotyledons (175 µm in length) of torpedo embryos. Arrowheads indicate polarized localization of PIN1-GFP in pre-procambial/procambial cells of wild type cotyledons. Red arrowheads indicate pre-procambial cells with incomplete PIN1 polarization. (J) Analysis of PIN1-GFP localization and cell elongation in developing basal strands of wild-type and *vcc* cotyledons at two developmental stages. Bar graphs show the percentage of embryonic cotyledons with polarized PIN1 in developing basal strands, elongating pre-procambial cells in basal strands, and PIN1 localization in vacuoles in basal strands (Col-0, n=35 and 44, and *vcc*, n=22 and 39 in 120-160 and 160-200 µm-long cotyledons, respectively). Scale bars: 10 µm (A); 5 µm (C,G); 20 µm (F,I).

Reduced vein network complexity in cotyledons of *vcc* mutants is caused by the reduction in basal vein formation. We found a correlation between the origin of basal veins and the position of the middle junction (Fig. 1D). In embryonic cotyledons, when the basal strand originates from the first PIN1 domain, the middle junction tends to locate at a more distal position than when it originates from the second PIN1 domain (Fig. 2E). Both patterns of basal strand initiation occur normally in *vcc* embryonic cotyledons (Fig. 4D). However, basal strands derived from the second PIN1 domain frequently fail to extend upwards and merge with the pre-existing distal strand in *vcc* (Fig. 4D,F). Consequently, the emerging basal strand remains isolated from pre-existing strands and eventually disappears without forming procambial cells (Fig. 4F). This isolated domain of pre-procambial cells may not be able to establish enough auxin flow to initiate procambial formation. According to this observation, we hypothesize that the middle junction and merging positions are located at significantly more distal positions in *vcc* cotyledons because basal strands originated from the second PIN1 domain frequently fail to specify procambial/vascular cells, and therefore, most of the basal veins in *vcc* mutant cotyledons derive from the first PIN1 domain (Fig. 10A).

Our analysis of 3xYFP- or tdTomato-tagged proteins indicate that VCC localizes to the plasma membrane of root and embryonic cells (Fig. 7C). This is inconsistent with a previous study reporting VCC localization at the endoplasmic reticulum of root cells (Wilson-Sánchez et al., 2018). However, this discrepancy could be explained by the level of expression in both systems as Wilson-Sánchez et al. (2018) and colleagues used the constitutive *CamV35S* promoter to drive VCC-CFP expression, whereas we used the native promoter region. We also observed that VCC is partially colocalized with PIN1 at the plasma membrane (Fig. 9H). In the *vcc* mutant embryonic cotyledons, PIN1 is expressed in pre-procambial cells during lateral strand formation (Fig. 9I). However, the strong polarization of PIN1 that precedes pre-procambial cell elongation and transition into procambial cell fate does not proceed normally in the *vcc* mutant. In addition, whereas in wild-type cotyledons PIN1 together with VCC are targeted to the vacuole for degradation in elongated procambial cells (Fig. 9A,D), PIN1 seems to prematurely undergo vacuolar sequestration in pre-procambial cells (Fig. 9J). Thus, the failed transition from pre-procambial to procambial cells in the *vcc* mutant seems to be connected to incomplete polarization of PIN1 and its premature degradation in the vacuole (Fig. 10B).

Both PIN1 polarization and its turnover in the vacuolar lumen require endocytic internalization and endosomal trafficking (Kleine-Vehn et al., 2011). The localization of VCC at the cell surface is consistent with a role stabilizing the localization of PIN1 at the plasma membrane. VCC shares similarities with the testraspanin proteins, such as their general topology and the

Development (2021) 148, dev197210. doi:10.1242/dev.197210

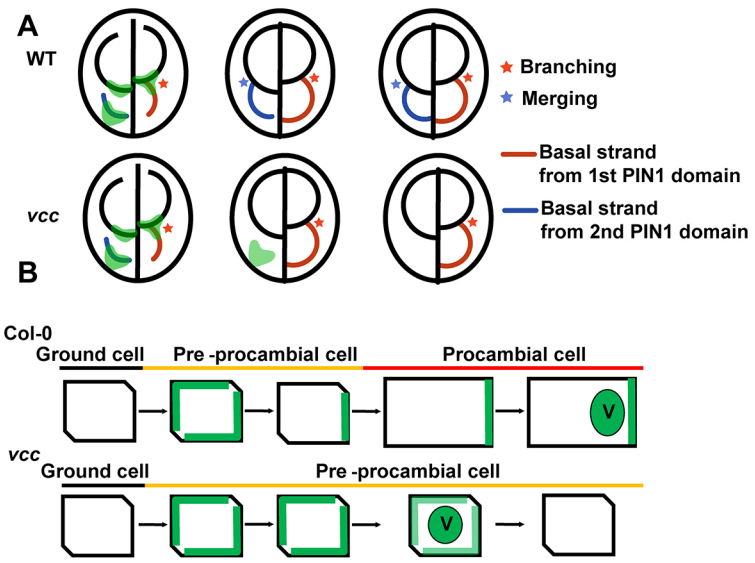

Fig. 10. Models of basal strand formation in wild type and *vcc*. (A) Model of basal strand formation in wild-type (WT) and *vcc* cotyledons. The establishment of the first and second PIN1 domains, and the initiation of basal strands, proceeds similarly in wild type and the *vcc* mutant. In wild-type cotyledons, the basal strand originated from the second PIN1 domain extends and merges with the distal strand. In the *vcc* mutant, the pre-procambial cells at the second PIN1 domain fail to elongate and remain as an isolated incipient strand. These isolated basal strands eventually disappear without forming procambial cells. As a result, only basal strands branched out from the first PIN1 domain remain in *vcc* cotyledons, leading to a drastic reduction in vein network complexity. (B) Model of pre-procambial/procambial cell specification in wild type and *vcc*. PIN1 (green) is initially expressed and localized at the plasma membrane of pre-procambial cells in both wild-type and *vcc* mutant cotyledons. In wild type, PIN1 becomes polarized, leading to cell elongation and procambial cell formation. Upon pre-procambial cell elongation, a large pool of PIN1 is transported to vacuoles (V) for degradation. In *vcc* mutant cotyledons, PIN1 fails to polarize in pre-procambial cells and it is prematurely delivered to vacuoles, resulting in defects in the procambial specification.

presence of charged amino acids in transmembrane domains (Roschzttardtz et al., 2014). Tetraspanins are evolutionarily conserved integral proteins that facilitate the assembly of protein networks in membranes (Charrin et al., 2009; Rubinstein, 2011; Wang et al., 2012). By interacting with each other, testraspanins form large networks called ‘tetraspanin webs’ (Hemsley et al., 2013) that cluster together receptors and signaling components to specific sites of membranes enriched in sterols. PIN1 is known to localize to sterol-rich detergent-resistant membrane domains (Titapiwatanakun et al., 2009), and VCC could be required to either form these membrane domains or to retain PIN1 in them. Interestingly, the auxin transporter ATP-BINDING CASSETTE TRANSPORTER B19 (ABCB19) is another protein that has been proposed to stabilize PIN1 in sterol-rich domains (Titapiwatanakun et al., 2009). Similar to VCC, ABCB19 becomes predominantly expressed in procambial cells during embryonic cotyledon development and is redirected from the plasma membrane to vacuoles (Lewis et al., 2009). The *abcb19* mutants showed abnormal auxin distribution in developing embryonic cotyledons (Lewis et al., 2009), but how much of this defect is due to a direct effect on its own auxin transport activity or on the stability of PIN1 at the plasma membrane is currently unclear. The role of VCC on PIN1 stabilization/localization seems to be crucial during the specification of procambial strands in embryonic cotyledons but not in vascular development after germination as the *vcc* mutant shows normal vein development in roots and aerial organs. This could be attributed to either redundancy within the fifteen members of the DUF1218 protein family to which VCC belongs, or to a special requirement for PIN1 stabilization during procambial cell fate specification in lateral strands in embryonic cotyledons.

MATERIALS AND METHODS

Plant materials and growth conditions

Arabidopsis thaliana ecotype Col-0 was used as wild-type control unless otherwise stated. Seeds were stratified at 4°C in the dark for 2 days and grown on half-strength Murashige and Skoog (MS) medium with 1% sucrose (w/v) and 0.8% agar (w/v) for 1-2 weeks at 22°C under 16-h light/8-h dark cycles, and then transferred to soil. Single mutant lines were described previously: *vcc-3* (SAIL_237_C09; Roschzttardtz et al., 2014); *pin1-1* (Okada et al., 1991; Belteton et al., 2018); and *pid-14* (SALK_049736; Dhonukshe et al., 2010). The *vcc-3 pin1-1* double mutant was generated by crossing.

Plasmid construction and transgenic lines

The lines expressing *pPIN1::PIN1-GFP* (CS9362; Benková et al., 2003) and VAMP711-mCherry (CS781673; Geldner et al., 2009) were obtained from the *Arabidopsis* Biological Resource Center.

To generate 3xYPET- or tdTomato-tagged VCC, the coding sequence of 3xYPET or tdTomato was placed immediately after the start codon of *VCC* in the KAZUSA transformation-competent artificial chromosome K17G15 by recombineering (Yanagisawa et al., 2018; Brumos et al., 2020). Recombineering primers were as follows: VCC-REC-N-F, 5′-AAGTATCTCCAACAAAACTAAATCCTACTAAGTTAAGAGATTTGAAAATGGGAGGTGGAGGTGGAGCT-3′, and VCC-REC-N-R, 5′-ACATCTAAGCCCACAATGACTAGACAAACAAGAATACCTCCTATCTTTGTGGCCCCAGCGGCCGCAGCAGCACC-3′. For generation of the CRISPR/Cas9-edited lines *pid-17* and *vcc pid-18*, the gRNA adaptor from PID-CRP1-F 5′-ATTGCGGCGCCGATACGACGCATG-3′ and PID-CRP1-R 5′-AAACCATGCGTCGTATCGGCGCCG-3′ was inserted into the egg cell-specific CRISPR/Cas9 vector pHEE401E (Wang et al., 2015). The resulting constructs were sequence verified and transformed into *Agrobacterium* GV3101, and then into *Arabidopsis*. Hygromycin-resistant T1 plants were screened for editing by FatI digestion of the PCR products using the following primers: *pid-14* LP, 5′-ATGTTACGAGAATCAGACGGTG-3′ and PID-R1, 5′-TAAATCACCACCGGAGCAAT-3′. Four independent lines were further verified by sequencing, and T2 progeny of all four lines showed seedlings with three cotyledons.

Cotyledon shape and vein pattern analysis

Cotyledons were removed from 7-day-after-germination or older seedlings, and incubated in 95% ethanol for 2 h or longer to remove chlorophyll and other cellular contents. Cleared cotyledons were imaged using a Nikon SMZ1500 dissecting microscope. More than 100 cotyledons per genotype were scored for vein patterns. Mutants for *vcc* and *pin1-1* were in Col-0 and En-1 wild-type background. To reduce the effect resulting from different ecotype backgrounds, we isolated single mutant lines from the mixture of Col-0 and En-1 background after crossing. Homozygous *pin1-1* mutants were identified by the presence of one or three cotyledons, fused cotyledons or leaves, and abnormal phyllotaxis. As only 10% of the progeny from *PIN1/pin1-1* (n=635) and *vcc PIN1/pin1-1* (n=732) plants showed abnormal cotyledons or leaves, the remaining plants were grown longer to observe the pin-like inflorescent meristem typical of *pin1-1* mutants; the cotyledons of these older plants were analyzed. Homozygous *pid* mutants were identified as seedlings with three cotyledons, representing 23% and 26% of the progeny from *PID/pid-17* (n=448) and *vcc PID/pid-18* (n=363) plants, respectively. For *vcc* and Col-0, we calculated cotyledon shape parameters using ImageJ based on circularity=4π area/perimeter^2 and roundness=4area/(π length^2).

Development (2021) 148, dev197210. doi:10.1242/dev.197210

Statistical analysis

Statistical tests were performed using R software (www.r-project.org/). The Shapiro–Wilk test was used to determine normality. *P*-values of χ^2 tests for more than two populations were adjusted by a false discovery rate method (Benjamini and Hochberg, 1995) to reduce type I error.

Confocal microscopy

Fluorescent images were acquired using a Zeiss LSM 780 inverted microscope with a 20× Plan-Apo 0.8 NA or a 40× C-Apo 1.1 NA water-immersion objective lens. GFP was excited by a 488 nm laser line with collection window set to 493-556 nm. YPET and FM4-64 were excited with a 514 nm laser and collected using 519-583 and 624-739 nm windows, respectively. Propidium iodide, mCherry and tdTomato were excited with a 561 nm laser and detected at 588-705 nm, 583-664 nm and 566-624 nm, respectively. Calcofluor white was excited with a 405 nm laser and emission collected at 425-474 nm. Image analysis and quantification were performed using ImageJ (http://imagej.nih.gov/ij/).

Embryo imaging

Embryos expressing fluorescent proteins were isolated from developing seeds using a dissecting microscope. Isolated embryos were placed in 30-50 µl drops of water in an 18-well microscope slide (Ibidi). For imaging, globular and torpedo embryos were kept in the microscope well and early bent-cotyledon embryos were transferred between two cover glasses. Cell wall staining was performed according to the ClearSee protocol (Ursache et al., 2018). Briefly, isolated embryos were fixed with 4% paraformaldehyde for 1 h and then cleared in the ClearSee solution containing 10% xylitol, 15% sodium deoxycholate and 25% urea for 24 h. Cleared embryos were stained with 0.1% calcofluor white (Sigma-Aldrich) for 1 h before imaging.

Fluorescence signal intensity profiles

For the peak intensity analysis, signal intensity was measured along lines using the plot profile function in ImageJ. Single optical sections showing plasma membrane or mid-planes of vacuoles were selected for the analysis. Relative intensity was determined by the equation:

$$(X^{\text{intensity}} - \text{minimum}^{\text{intensity}})/(\text{maximum}^{\text{intensity}} - \text{minimum}^{\text{intensity}}).$$

Basal strand analysis

Images of embryonic cotyledons expressing PIN1-GFP were used for the analysis. The first and second PIN1 domains were determined by the presence or absence of a connection with the distal strand in 120- to 160-µm-long cotyledons, respectively. Elongated procambial cells were defined as those with a length that was at least 1.5× longer than their width.

RT-PCR and RT-qPCR

Wild-type plants were vertically grown on half-strength MS medium containing 1% sucrose and 0.8% agar. At 12 days after germination, seedlings were transferred onto a new half-strength MS plate containing 0.1% ethanol or 10 µM NAA for 24 h. For RT-PCR, total RNA was extracted from seedlings using TRIzol (Ambion). cDNA was synthesized using a High-Capacity cDNA Reverse Transcription Kit (Applied Biosystems), followed by PCR with gene specific primers: VCC-RT-F1, 5′-CGCCCAAAATCAGGTGAAG-3′; VCC-RT-R1, 5′-CCCAAATC-CAACAGCGAATAC-3′; ACT2-F1, 5′-TCCCAGTGTTGTTGGTAGGC-3′; and ACT2-R1, 5′-CACGTCCAGCAAGGTCAAGA-3′. *VCC* and *ACT2* were amplified through 32 and 28 cycles, respectively. For RT-qPCR, seedlings were harvested after 2 and 24 h after the auxin treatment, and flash-frozen in liquid nitrogen. The 1600 MiniG tissue homogenizer (SPEX SamplePrep) was used to grind frozen tissue. Total RNA was extracted using TRIzol reagent and following manufacturer's instructions. RNA quantification and integrity were determined using a NanoDrop 2000 spectrophotometer (Thermo Fisher Scientific). Residual DNA contamination was removed using DNAse I (AMPDI; Sigma-Aldrich). RT-qPCR analysis was performed using the Luna Universal One-Step RT-qPCR kit (New England BioLabs) in a 7500 Real Time PCR System (Applied Biosystems). Transcript levels of *VCC*, *PIN1* and *UBIQUITIN 10* (*UBQ10*) were quantified using the following primers: VCC-qPCR-F4, 5′-TCCTCGGAATCCAAGCTGAAG-3′, and VCC-qPCR-R4, 5′-AAGAC-AGCCTCCGACCAAG-3′ for *VCC*; PIN1-qPCR-F1, 5′-ACAAAACGA-CGCAGGCTAAG-3′, and PIN1-qPCR-R1, 5′-AGCTGGCATTTCAA-TGTTCC-3′ for *PIN1*; and UBQ10-F 5′-CACACTCCACTTGGTCT-TGCGT-3′, and UBQ10-R 5′-TGGTCTTTCCGGTGAGAGTCTTCA-3′ for *UBQ10*. The expression levels of *VCC* and *PIN1* were normalized by the *UBQ10* expression level.

Acknowledgements

We thank Enrico Scarpella (University of Alberta) for providing the *pATHB8::NLS-YFP* line and Cecile Ané (University of Wisconsin-Madison) for her support with statistical analyses.

Competing interests

The authors declare no competing or financial interests.

Author contributions

Conceptualization: M.Y., M.S.O.; Methodology: M.Y.; Validation: M.Y.; Formal analysis: M.Y., A.P., M.S.O.; Investigation: M.Y., A.P.; Resources: M.S.O.; Writing - original draft: M.Y., M.S.O.; Writing - review & editing: M.Y., A.P., M.S.O.; Visualization: M.Y., M.S.O.; Supervision: M.S.O.; Project administration: M.S.O.; Funding acquisition: M.S.O.

Funding

This work was supported by the National Science Foundation (NSF IOS 1457123 to M.S.O.). A.P. was supported by the Institut National de la Recherche Agronomique (France) and the National Science Foundation (NSF IOS 1557899).

Peer review history

The peer review history is available online at https://journals.biologists.com/dev/article-lookup/doi/10.1242/dev.197210

References

Aida, M., Vernoux, T., Furutani, M., Traas, J. and Tasaka, M. (2002) Roles of PIN-FORMED1 and MONOPTEROS in pattern formation of the apical region of the Arabidopsis embryo. *Development* **129**, 3965-3974.

Anne, P., Azzopardi, M., Gissot, L., Beaubiat, S., Hématy, K. and Palauqui, J.-C. (2015). OCTOPUS negatively regulates BIN2 to control phloem differentiation in *Arabidopsis thaliana*. *Curr. Biol.* **25**, 2584-2590. doi:10.1016/j.cub.2015.08.033

Belteton, S. A., Sawchuk, M. G., Donohoe, B. S., Scarpella, E. and Szymanski, D. B. (2018). Reassessing the roles of PIN proteins and anticlinal microtubules during pavement cell morphogenesis. *Plant Physiol.* **176**, 432-449. doi:10.1104/pp.17.01554

Benjamini, Y. and Hochberg, Y. (1995). Controlling the false discovery rate: a practical and powerful approach to multiple testing. *J. R. Statist. Soc.* **57**, 289-300. doi:10.1111/j.2517-6161.1995.tb02031.x

Benjamins, R., Quint, A., Weijers, D., Hooykaas, P. and Offringa, R. (2001). The PINOID protein kinase regulates organ development in *Arabidopsis* by enhancing polar auxin transport. *Development* **128**, 4057-4067. doi:10.1242/dev.128.20.4057

Benková, E., Michniewicz, M., Sauer, M., Teichmann, T., Seifertová, D., Jürgens, G. and Friml, J. (2003). Local, efflux-dependent auxin gradients as a common module for plant organ formation. *Cell* **115**, 591-602. doi:10.1016/S0092-8674(03)00924-3

Berleth, T. and Jurgens, G. (1993). The role of the monopteros gene in organising the basal body region of the *Arabidopsis* embryo. *Development* **118**, 575-587. doi:10.1242/dev.118.2.575

Bhatia, N., Bozorg, B., Larsson, A., Ohno, C., Jönsson, H. and Heisler, M. G. (2016). Auxin acts through MONOPTEROS to regulate plant cell polarity and pattern phyllotaxis. *Curr. Biol.* **26**, 3202-3208. doi:10.1016/j.cub.2016.09.044

Boer, D. R., Freire-Rios, A., van den Berg, W. A. M., Saaki, T., Manfield, I. W., Kepinski, S., López-Vidrieo, I., Franco-Zorrilla, J. M., de Vries, S. C., Solano, R. et al. (2014). Structural basis for DNA binding specificity by the auxin-dependent ARF transcription factors. *Cell* **156**, 577-589. doi:10.1016/j.cell.2013.12.027

Breda, A. S., Hazak, O., Schultz, P., Anne, P., Graeff, M., Simon, R. and Hardtke, C. S. (2019). A cellular insulator against CLE45 peptide signaling. *Curr. Biol.* **29**, 2501-2508.e3. doi:10.1016/j.cub.2019.06.037

Brumos, J., Zhao, C., Gong, Y., Soriano, D., Patel, A. P., Perez-Amador, M. A., Stepanova, A. N. and Alonso, J. M. (2020). An improved recombineering toolset for plants. *Plant Cell* **32**, 100-122. doi:10.1105/tpc.19.00431

Carland, F. and Nelson, T. (2009). CVP2- and CVL1-mediated phosphoinositide signaling as a regulator of the ARF GAP SFC/VAN3 in establishment of foliar vein patterns. *Plant J.* **59**, 895-907. doi:10.1111/j.1365-313X.2009.03920.x

Carland, F. M., Berg, B. L., FitzGerald, J. N., Jinamornphongs, S., Nelson, T. and Keith, B. (1999). Genetic regulation of vascular tissue patterning in *Arabidopsis*. *Plant Cell* **11**, 2123-2137. doi:10.1105/tpc.11.11.2123

Carland, F. M., Fujioka, S., Takatsuto, S., Yoshida, S. and Nelson, T. (2002). The identification of CVP1 reveals a role for sterols in vascular patterning. *Plant Cell* **14**, 2045-2058. doi:10.1105/tpc.003939

Charrin, S., le Naour, F., Silvie, O., Milhiet, P.-E., Boucheix, C. and Rubinstein, E. (2009). Lateral organization of membrane proteins: tetraspanins spin their web. *Biochem. J.* **420**, 133-154. doi:10.1042/BJ20082422

Christensen, S. K., Dagenais, N., Chory, J. and Weigel, D. (2000). Regulation of auxin response by the protein kinase PINOID. *Cell* **100**, 469-478. doi:10.1016/S0092-8674(00)80682-0

De Rybel, B., Möller, B., Yoshida, S., Grabowicz, I., Barbier de Reuille, P., Boeren, S., Smith, R. S., Borst, J. W. and Weijers, D. (2013). A bHLH complex controls embryonic vascular tissue establishment and indeterminate growth in *Arabidopsis*. *Dev. Cell* **24**, 426-437. doi:10.1016/j.devcel.2012.12.013

De Rybel, B., Adibi, M., Breda, A. S., Wendrich, J. R., Smit, M. E., Novák, O., Yamaguchi, N., Yoshida, S., Van Isterdael, G., Palovaara, J. et al. (2014). Integration of growth and patterning during vascular tissue formation in *Arabidopsis*. *Science* **345**, 1255215. doi:10.1126/science.1255215

Dhonukshe, P., Huang, F., Galvan-Ampudia, C. S., Mähönen, A. P., Kleine-Vehn, J., Xu, J., Quint, A., Prasad, K., Friml, J., Scheres, B. et al. (2010). Plasma membrane-bound AGC3 kinases phosphorylate PIN auxin carriers at TPRXS(N/S) motifs to direct apical PIN recycling. *Development* **137**, 3245-3255. doi:10.1242/dev.052456

Friml, J., Yang, X., Michniewicz, M., Weijers, D., Quint, A., Tietz, O., Benjamins, R., Ouwerkerk, P. B. F., Ljung, K., Sandberg, G. et al. (2004). A PINOID-dependent binary switch in apical-basal PIN polar targeting directs auxin efflux. *Science* **306**, 862-865. doi:10.1126/science.1100618

Geldner, N., Anders, N., Wolters, H., Keicher, J., Kornberger, W., Muller, P., Delbarre, A., Ueda, T., Nakano, A. and Jürgens, G. (2003). The *Arabidopsis* GNOM ARF-GEF mediates endosomal recycling, auxin transport, and auxin-dependent plant growth. *Cell* **112**, 219-230. doi:10.1016/S0092-8674(03)00003-5

Geldner, N., Dénervaud-Tendon, V., Hyman, D. L., Mayer, U., Stierhof, Y.-D. and Chory, J. (2009). Rapid, combinatorial analysis of membrane compartments in intact plants with a multicolor marker set. *Plant J.* **59**, 169-178. doi:10.1111/j.1365-313X.2009.03851.x

Haga, K., Hayashi, K.-i. and Sakai, T. (2014). PINOID AGC kinases are necessary for phytochrome-mediated enhancement of hypocotyl phototropism in *Arabidopsis*. *Plant Physiol.* **166**, 1535. doi:10.1104/pp.114.244434

Hamann, T., Benkova, E., Bäurle, I., Kientz, M. and Jürgens, G. (2002). The Arabidopsis *BODENLOS* gene encodes an auxin response protein inhibiting *MONOPTEROS*-mediated embryo patterning. *Genes Dev.* **16**, 1610-1615. doi:10.1101/gad.229402

Hardtke, C. S. and Berleth, T. (1998). The Arabidopsis gene *MONOPTEROS* encodes a transcription factor mediating embryo axis formation and vascular development. *EMBO J.* **17**, 1405-1411. doi:10.1093/emboj/17.5.1405

Hemsley, P. A., Weimar, T., Lilley, K. S., Dupree, P. and Grierson, C. S. (2013). A proteomic approach identifies many novel palmitoylated proteins in *Arabidopsis*. *New Phytol.* **197**, 805-814. doi:10.1111/nph.12077

Hobbie, L., McGovern, M., Hurwitz, L. R., Pierro, A., Liu, N. Y., Bandyopadhyay, A. and Estelle, M. (2000). The *axr6* mutants of *Arabidopsis thaliana* define a gene involved in auxin response and early development. *Development* **127**, 23-32. doi:10.1242/dev.127.1.23

Hou, H., Erickson, J., Meservy, J. and Schultz, E. A. (2010). *FORKED1* encodes a PH domain protein that is required for PIN1 localization in developing leaf veins. *Plant J.* **63**, 960-973. doi:10.1111/j.1365-313X.2010.04291.x

Izhaki, A. and Bowman, J. L. (2007). KANADI and class III HD-Zip gene families regulate embryo patterning and modulate auxin flow during embryogenesis in *Arabidopsis*. *Plant Cell* **19**, 495-508. doi:10.1105/tpc.106.047472

Kleine-Vehn, J., Huang, F., Naramoto, S., Zhang, J., Michniewicz, M., Offringa, R. and Friml, J. (2009). PIN auxin efflux carrier polarity is regulated by PINOID kinase-mediated recruitment into GNOM-independent trafficking in *Arabidopsis*. *Plant Cell* **21**, 3839-3849. doi:10.1105/tpc.109.071639

Kleine-Vehn, J., Wabnik, K., Martinière, A., Łangowski, L., Willig, K., Naramoto, S., Leitner, J., Tanaka, H., Jakobs, S., Robert, S. et al. (2011). Recycling, clustering, and endocytosis jointly maintain PIN auxin carrier polarity at the plasma membrane. *Mol. Syst. Biol.* **7**, 540. doi:10.1038/msb.2011.72

Koizumi, K., Sugiyama, M. and Fukuda, H. (2000). A series of novel mutants of *Arabidopsis thaliana* that are defective in the formation of continuous vascular network: calling the auxin signal flow canalization hypothesis into question. *Development* **127**, 3197-3204. doi:10.1242/dev.127.15.3197

Koizumi, K., Naramoto, S., Sawa, S., Yahara, N., Ueda, T., Nakano, A., Sugiyama, M. and Fukuda, H. (2005). VAN3 ARF–GAP-mediated vesicle transport is involved in leaf vascular network formation. *Development* **132**, 1699-1711. doi:10.1242/dev.01716

Lewis, D. R., Wu, G., Ljung, K. and Spalding, E. P. (2009). Auxin transport into cotyledons and cotyledon growth depend similarly on the ABCB19 Multidrug Resistance-like transporter. *Plant J.* **60**, 91-101. doi:10.1111/j.1365-313X.2009.03941.x

Lucas, W. J., Groover, A., Lichtenberger, R., Furuta, K., Yadav, S.-R., Helariutta, Y., He, X.-Q., Fukuda, H., Kang, J., Brady, S. M. et al. (2013). The plant vascular system: evolution, development and functions. *J. Integr. Plant Biol.* **55**, 294-388. doi:10.1111/jipb.12041

Marhavý, P., Bielach, A., Abas, L., Abuzeineh, A., Duclercq, J., Tanaka, H., Pařezová, M., Petrášek, J., Friml, J., Kleine-Vehn, J. et al. (2011). Cytokinin modulates endocytic trafficking of PIN1 auxin efflux carrier to control plant organogenesis. *Dev. Cell* **21**, 796-804. doi:10.1016/j.devcel.2011.08.014

Marhavý, P., Duclercq, J., Weller, B., Feraru, E., Bielach, A., Offringa, R., Friml, J., Schwechheimer, C., Murphy, A. and Benková, E. (2014). Cytokinin controls polarity of PIN1-dependent auxin transport during lateral root organogenesis. *Curr. Biol.* **24**, 1031-1037. doi:10.1016/j.cub.2014.04.002

Mewalal, R., Mizrachi, E., Coetzee, B., Mansfield, S. D. and Myburg, A. A. (2016). The *Arabidopsis* domain of unknown function 1218 (DUF1218) containing proteins, MODIFYING WALL LIGNIN-1 and 2 (At1g31720/MWL-1 and At4g19370/MWL-2) function redundantly to alter secondary cell wall lignin content. *PLoS ONE* **11**, e0150254. doi:10.1371/journal.pone.0150254

Mironova, V. V., Omelyanchuk, N. A., Wiebe, D. S. and Levitsky, V. G. (2014). Computational analysis of auxin responsive elements in the *Arabidopsis thaliana* L. genome. *BMC Genomics* **15**, S4. doi:10.1186/1471-2164-15-S12-S4

Möller, B. K., ten Hove, C. A., Xiang, D., Williams, N., López, L. G., Yoshida, S., Smit, M., Datla, R. and Weijers, D. (2017). Auxin response cell-autonomously controls ground tissue initiation in the early *Arabidopsis* embryo. *Proc. Natl. Acad. Sci. USA* **114**, E2533-E2539. doi:10.1073/pnas.1616493114

Naramoto, S., Sawa, S., Koizumi, K., Uemura, T., Ueda, T., Friml, J., Nakano, A. and Fukuda, H. (2009). Phosphoinositide-dependent regulation of VAN3 ARF-GAP localization and activity essential for vascular tissue continuity in plants. *Development* **136**, 1529-1538. doi:10.1242/dev.030098

Ohashi-Ito, K. and Bergmann, D. C. (2007). Regulation of the *Arabidopsis* root vascular initial population by LONESOME HIGHWAY. *Development* **134**, 2959-2968. doi:10.1242/dev.006296

Ohashi-Ito, K. and Fukuda, H. (2014). Initiation of vascular development. *Physiol. Plant* **151**, 142-146. doi:10.1111/ppl.12111

Ohashi-Ito, K., Oguchi, M., Kojima, M., Sakakibara, H. and Fukuda, H. (2013). Auxin-associated initiation of vascular cell differentiation by LONESOME HIGHWAY. *Development* **140**, 765-769. doi:10.1242/dev.087924

Ohashi-Ito, K., Iwamoto, K., Nagashima, Y., Kojima, M., Sakakibara, H. and Fukuda, H. (2019). A positive feedback loop comprising LHW-TMO5 and local auxin biosynthesis regulates initial vascular development in *Arabidopsis* roots. *Plant Cell Physiol.* **60**, 2684-2691. doi:10.1093/pcp/pcz156

Okada, K., Ueda, J., Komaki, M. K., Bell, C. J. and Shimura, Y. (1991). Requirement of the auxin polar transport system in early stages of *Arabidopsis* floral bud formation. *Plant Cell* **3**, 677-684. doi:10.2307/3869249

Ploense, S. E., Wu, M.-F., Nagpal, P. and Reed, J. W. (2009). A gain-of-function mutation in IAA18 alters *Arabidopsis* embryonic apical patterning. *Development* **136**, 1509-1517. doi:10.1242/dev.025932

Roschzttardtz, H., Paez-Valencia, J., Dittakavi, T., Jali, S., Reyes, F. C., Baisa, G., Anne, P., Gissot, L., Palauqui, J.-C., Masson, P. H. et al. (2014). The *VASCULATURE COMPLEXITY AND CONNECTIVITY* gene encodes a plant-specific protein required for embryo provasculature development. *Plant Physiol.* **166**, 889-902. doi:10.1104/pp.114.246314

Rubinstein, E. (2011). The complexity of tetraspanins. *Biochem. Soc. Trans.* **39**, 501-505. doi:10.1042/BST0390501

Sawchuk, M. G., Head, P., Donner, T. J. and Scarpella, E. (2007). Time-lapse imaging of *Arabidopsis* leaf development shows dynamic patterns of procambium formation. *New Phytol.* **176**, 560-571. doi:10.1111/j.1469-8137.2007.02193.x

Scarpella, E., Marcos, D., Friml, J. and Berleth, T. (2006). Control of leaf vascular patterning by polar auxin transport. *Genes Dev.* **20**, 1015-1027. doi:10.1101/gad.1402406

Sieburth, L. E. (1999). Auxin is required for leaf vein pattern in *Arabidopsis*. *Plant Physiol.* **121**, 1179-1190. doi:10.1104/pp.121.4.1179

Sieburth, L. E., Muday, G. K., King, E. J., Benton, G., Kim, S., Metcalf, K. E., Meyers, L., Seamen, E. and Van Norman, J. M. (2006). *SCARFACE* encodes an ARF-GAP that is required for normal auxin efflux and vein patterning in *Arabidopsis*. *Plant Cell* **18**, 1396-1411. doi:10.1105/tpc.105.039008

Smet, W., Sevilem, I., de Luis Balaguer, M. A., Wybouw, B., Mor, E., Miyashima, S., Blob, B., Roszak, P., Jacobs, T. B., Boekschoten, M. et al. (2019). DOF2.1 controls cytokinin-dependent vascular cell proliferation downstream of TMO5/LHW. *Curr. Biol.* **29**, 520-529.e6. doi:10.1016/j.cub.2018.12.041

Steinmann, T., Geldner, N., Grebe, M., Mangold, S., Jackson, C. L., Paris, S., Gälweiler, L., Palme, K. and Jurgens, G. (1999). Coordinated polar localization of auxin efflux carrier PIN1 by GNOM ARF GEF. *Science* **286**, 316-318. doi:10.1126/science.286.5438.316

Steynen, Q. J. and Schultz, E. A. (2003). The *FORKED* genes are essential for distal vein meeting in Arabidopsis. *Development* **130**, 4695-4708. doi:10.1242/dev.00689

Titapiwatanakun, B., Blakeslee, J. J., Bandyopadhyay, A., Yang, H., Mravec, J., Sauer, M., Cheng, Y., Adamec, J., Nagashima, A., Geisler, M. et al. (2009). ABCB19/PGP19 stabilises PIN1 in membrane microdomains in *Arabidopsis*. *Plant J.* **57**, 27-44. doi:10.1111/j.1365-313X.2008.03668.x

Truernit, E., Bauby, H., Belcram, K., Barthélémy, J. and Palauqui, J.-C. (2012). OCTOPUS, a polarly localised membrane-associated protein, regulates phloem differentiation entry in *Arabidopsis thaliana*. *Development* **139**, 1306-1315. doi:10.1242/dev.072629

Ubeda-Tomas, S., Edvardsson, E., Eland, C., Singh, S. K., Zadik, D., Aspeborg, H., Gorzsàs, A., Teeri, T. T., Sundberg, B., Persson, P. et al. (2007). Genomic-assisted identification of genes involved in secondary growth in *Arabidopsis* utilising transcript profiling of poplar wood-forming tissues. *Physiol. Plant* **129**, 415-428. doi:10.1111/j.1399-3054.2006.00817.x

Ulmasov, T., Liu, Z. B., Hagen, G. and Guilfoyle, T. J. (1995). Composite structure of auxin response elements. *Plant Cell* **7**, 1611-1623. doi:10.1105/tpc.7.10.1611

Ursache, R., Andersen, T. G., Marhavý, P. and Geldner, N. (2018). A protocol for combining fluorescent proteins with histological stains for diverse cell wall components. *Plant J.* **93**, 399-412. doi:10.1111/tpj.13784

Wang, F., Vandepoele, K. and Van Lijsebettens, M. (2012). Tetraspanin genes in plants. *Plant Sci.* **190**, 9-15. doi:10.1016/j.plantsci.2012.03.005

Wang, Z.-P., Xing, H.-L., Dong, L., Zhang, H.-Y., Han, C.-Y., Wang, X.-C. and Chen, Q.-J. (2015). Egg cell-specific promoter-controlled CRISPR/Cas9 efficiently generates homozygous mutants for multiple target genes in *Arabidopsis* in a single generation. *Genome Biol.* **16**, 144. doi:10.1186/s13059-015-0715-0

Wenzel, C. L., Schuetz, M., Yu, Q. and Mattsson, J. (2007). Dynamics of *MONOPTEROS* and *PIN-FORMED1* expression during leaf vein pattern formation in *Arabidopsis thaliana*. *Plant J.* **49**, 387-398. doi:10.1111/j.1365-313X.2006.02977.x

Wilson-Sánchez, D., Martínez-López, S., Navarro-Cartagena, S., Jover-Gil, S. and Micol, J. L. (2018). Members of the DEAL subfamily of the DUF1218 gene family are required for bilateral symmetry but not for dorsoventrality in *Arabidopsis* leaves. *New Phytol.* **217**, 1307-1321. doi:10.1111/nph.14898

Wiśniewska, J., Xu, J., Seifertová, D., Brewer, P. B., Růžička, K., Blilou, I., Rouquié, D., Benkova, E., Scheres, B. and Friml, J. (2006). Polar PIN localization directs auxin flow in plants. *Science* **312**, 883. doi:10.1126/science.1121356

Yanagisawa, M., Alonso, J. M. and Szymanski, D. B. (2018). Microtubule-dependent confinement of a cell signaling and actin polymerization control module regulates polarized cell growth. *Curr. Biol.* **28**, 2459-2466.e4. doi:10.1016/j.cub.2018.05.076

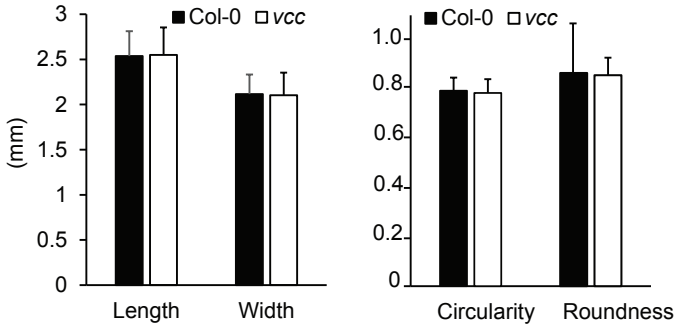

Fig. S1. Size and shape of wild-type and *vcc* cotyledons.(A) Length and width of cotyledons from seedlings of Col-0 and *vcc* at 8 days after germination. Mean + SD (n=100 cotyledons per genotype).
(B) Shape parameters circularity and roundness in wild-type and *vcc* cotyledons; Mean + SD (n = 100 cotyledons per genotype).

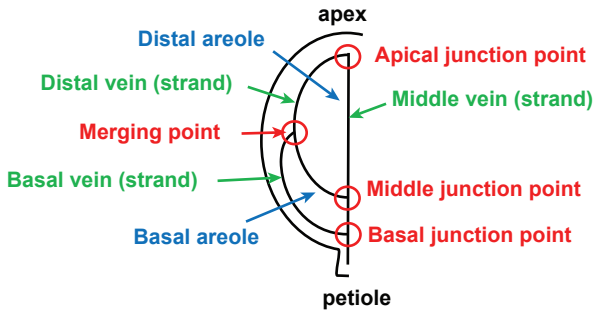

Fig. S2. Terminology to describe geometry of vein pattern in cotyle-dons.
The diagram indicates veins and vein merging points in half of an *Arabidopsis* cotyledon. An areole is the area enclosed by veins. The term “strand” denotes developing veins consisting of pre-procambial/procam-bial cells.

Development • Supplementary information

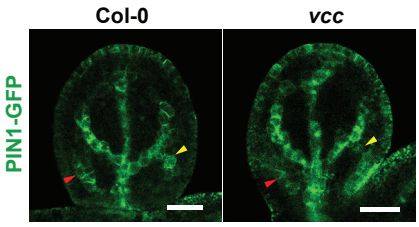

Fig. S3. Basal strand formation in wild type and *vcc* cotyledons. Basal strands originate from the first (yellow) or second (red) PIN1 domains in wild-type and *vcc* cotyledons (approximately 140 µm in length).
Scale bars = 30 µm.

Nucleotide sequence
PID
226 CGCCTCAT GCGTCGTATCGGCGCCGGCGACATCGGAACAGTTTAC 270
pid-17
226 CGCCTCATGGCGTCGTATCGGCGCCGGCGACATCGGAACAGTTTAC 271
pid-18
226 CGCCTCATTGCGTCGTATCGGCGCCGGCGACATCGGAACAGTTTAC 271

Deduced amino acid sequences
PID
76 RLMRRIGAGDIGTVY 90
PID-17
76 RLMASYRRRRHRNSL 90
PID-18
76 RLMASYRRRRHRNSL 90

Fig. S4. Identification of mutations in CRISPR/ CAS9-edited lines.
Nucleotide and deduced amino acid sequences of PID, *pid-17*, and *pid-18*. Under-lined nucleotides show the PAM sequence. Single nucleotide G and T (highlighted by red color) were inserted after the nucleotide 233 from the translation site in *pid-17* and *pid-18*, respectively. Predicted amino acid changes (highlighted in red) in PID-17 and PID-18 mutant proteins.

Development • Supplementary information

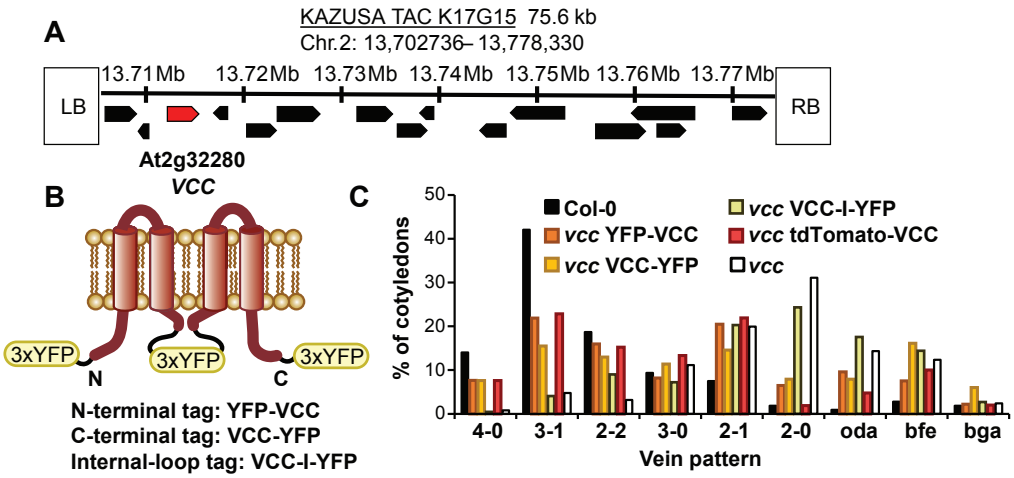

Fig. S5. Fluorescent protein-tagged VCC versions and rescue analysis.
(A) The KAZUSA TAC clone K17G15 contains the *VCC* genomic sequence. (B) Predicted structure of VCC at a membrane and positions of the 3x-YFP tag. (C) Rescue analysis of 3x-YFP- and tdTomato-tagged VCC in the *vcc* mutant back-ground. Average of three independent transgenic lines are shown, except for VCC-I-YFP for which two lines were analyzed.

Development • Supplementary information

Supplementary Table 1: Statistical analyses of vein network complexity and vein disconnections

Chi-squared test: vein network complexity (Fig 5a)		
Comparison	Raw P-value	Adjusted P-value
Col-0 vs En-1	0.2471	0.2745
Col-0 vs *vcc*	0.0001	0.0001
Col-0 vs *pin1-1*	0.0000	0.0001
Col-0 vs *vcc pin1-1*	0.0000	0.0000
En-1 vs *vcc*	0.0043	0.0071
En-1 vs *pin1-1*	0.0032	0.0064
En-1 vs *vcc pin1-1*	0.0000	0.0000
vcc vs *pin1-1*	0.8781	0.8781
vcc vs vcc *pin1-1*	0.0289	0.0414
pin1-1 vs vcc *pin1-1*	0.0541	0.0676

Chi-squared test: connectivity related (Fig 5a)		
Comparison	Raw P-value	Adjusted P-value
Col-0 vs En-1	0.1049	0.1748
Col-0 vs *vcc*	0.0008	0.0038
Col-0 vs *pin1-1*	0.0028	0.0092
Col-0 vs *vcc pin1-1*	0.0000	0.0003
En-1 vs *vcc*	0.0767	0.1533
En-1 vs *pin1-1*	0.1356	0.1938
En-1 vs *vcc pin1-1*	0.0065	0.0162
vcc vs *pin1-1*	0.8665	0.8665
vcc vs vcc *pin1-1*	0.3482	0.3869
pin1-1 vs vcc *pin1-1*	0.2573	0.3216

Chi-squared test: complexity (Fig 5b)		
Comparison	Raw P-value	Adjusted P-value
Col-0 vs *vcc*	0.0000	0.0000
Col-0 vs *pid-14*	0.0000	0.0000
Col-0 vs *pid-17*	0.0000	0.0000
Col-0 vs *vcc pid-18*	0.0000	0.0000
vcc vs *pid-14*	0.4684	0.5855
vcc vs *pid-17*	0.0553	0.1105
vcc vs *vcc pid-18*	0.7509	0.8343
pid-14 vs *pid-17*	0.2265	0.3775
pid-14 vs *vcc pid-18*	1.0000	1
pid-17 vs *vcc pid-18*	0.2992	0.4274

Chi-squared test: connectivity (Fig 5b)		
Comparison	Raw P-value	Adjusted P-value
Col-0 vs *vcc*	0.0001	0.0002
Col-0 vs *pid-14*	0.0000	0.0000
Col-0 vs *pid-17*	0.0044	0.0063
Col-0 vs *vcc pid-18*	0.0000	0.0000
vcc vs *pid-14*	0.6702	0.6702
vcc vs *pid-17*	0.3701	0.4112
vcc vs *vcc pid-18*	0.0000	0.0000
pid-14 vs *pid-17*	0.1442	0.1803
pid-14 vs *vcc pid-18*	0.0000	0.0000
pid-17 vs *vcc pid-18*	0.0000	0.0000

Development • Supplementary information